

# The Space-Time Structure and Variability of the Shelf Water–Slope Water and Gulf Stream Surface Temperature Fronts and Associated Warm-Core Eddies

GEORGE R. HALLIWELL, JR., AND CHRISTOPHER N. K. MOOERS

*College of Marine Studies, University of Delaware, Lewes, Delaware 19958*

The space-time structure and variability of three thermal features on the surface of the Northwest Atlantic—the shelf water–slope water front; the Gulf Stream front; and warm-core, anticyclonic eddies—were examined between September 1, 1975, and August 31, 1977, using weekly satellite-derived charts of surface temperature fronts. The temporal and spatial correlation scales of both the shelf-slope and Gulf Stream fronts were about 2 weeks and 80 km, respectively. The rms amplitude of both fronts increased from about 25 to 80 km in the first 1,000 km northeastward from Cape Hatteras. The dominant Gulf Stream meanders had wavelengths of about 320 km and periods of 7–8 weeks, and they propagated downstream at a speed of about 6 cm/s. The warm-core eddies averaged about 100 km in diameter and propagated southwestward from Georges Bank at an average speed of 6 cm/s; they decreased in diameter from about 120 to 90 km and increased in speed from about 4 to 7 cm/s in moving from the Georges Bank–to–Hudson Canyon subdomain to the Hudson Canyon–to–Cape Charles subdomain. Some large Gulf Stream meanders induced perturbations of the shelf-slope front. Eddies forced seaward perturbations of the front, which propagated southwestward with the eddies. (There were more rapidly propagating disturbances which also moved southwestward along the shelf-slope front; they may have been due to coastally trapped waves.) There was significant interannual variation in the mean position of the Gulf Stream front and the number and intensity of warm-core eddies shed by the Stream, though the correlation scales of its front did not change. Consequently, there were substantial interannual variations in the inferred entrainment of shelf waters by warm-core eddies. Furthermore, the correlation scales of the shelf-slope front had interannual variation. The results of this study agree with earlier, more limited estimates, and they extend the statistical analyses to the space-time continuum of long waves and meanders with the aid of wave number–frequency spectra and empirical orthogonal functions. These analyses quantify the broadband nature of the various perturbations and their interactions. Thus a holistic view of the principal surface thermal features of the Northwest Atlantic, and their interactions, is provided.

## INTRODUCTION

Satellite-derived data were used to analyze the temporal and spatial variability of the position of three surface thermal features of the Northwest Atlantic: the shelf water–slope water thermal boundary (hereafter referred to as the shelf-slope front); the Gulf Stream front; and the warm-core, anticyclonic eddies (hereafter referred to as the eddies) which are shed by the Gulf Stream and propagate southwestward along the shelfbreak from the general vicinity of Georges Bank. Surface position data were obtained from 2 years of weekly experimental ocean frontal analysis (EOFAs) charts produced by the *U.S. Naval Oceanographic Office* [1975–1977]; Figure 1 shows an example chart with our digitization grids superimposed. The surface temperature fronts (the shelf-slope and Gulf Stream fronts and the surface thermal boundaries of the eddies) are located on the EOFAs charts by using satellite thermal (infrared) imagery obtained from the very high resolution radiometer (VHRR) of the NOAA satellites, augmented with surface temperatures obtained by ships and aircraft. (The *Goes 1* satellite images, based on the visible and infrared spin scan radiometer (VISSR), are not used to prepare the EOFAs charts, owing to their low spatial resolution compared with the NOAA imagery.) The EOFAs charts are dated on Wednesday of each week; the 104 charts from September 3, 1975, through August 24, 1977, were used. They are constructed using surface temperature data from the week before the issue date and from satellite images as close as possible to this date. Surface temperatures from ships and aircraft are used to ver-

ify the positions of fronts obtained from the images and to quantify temperature differences across the fronts.

Following descriptions of the phenomena studied, the digitization procedures are outlined along with a discussion of important sources of error. The data analysis procedures are described, and then descriptions of the spatial and temporal structure and scales of the fronts and eddies, and their interactions, are presented.

## BACKGROUND

*Shelf-slope front.* In satellite thermal imagery the shelf-slope front is a continuous and persistent feature from the Middle Atlantic Shelf northeastward along the Scotian Shelf. It is the surface manifestation of a thermalhaline front, which is largely density compensated and which extends through the water column to the bottom of the Middle Atlantic Shelf [Flagg, 1977]. Between late spring and early autumn the temperature front is weak above the seasonal thermocline, but the cross-front temperature difference (usually less than 2°C) is usually detectable by the VHRR, which under ideal conditions can resolve a temperature change of about 0.5°C across a distance of 0.8 km. The front usually intersects the surface within 50 km offshore of the shelfbreak in the southwest and 150 km in the northeast. Beneath the surface it slopes downward and onshore, generally intersecting the bottom just shoreward of the shelfbreak and forming a bottom front here. From 1974 through 1976 the surface front was displaced as far as 100 km shoreward and 300 km seaward of the shelfbreak [Ingham, 1976; Gunn, 1979]. In contrast, Wright [1976] found the bottom front within 16 km of the shelfbreak 80% of the time. The present study focuses on the variability of the sur-

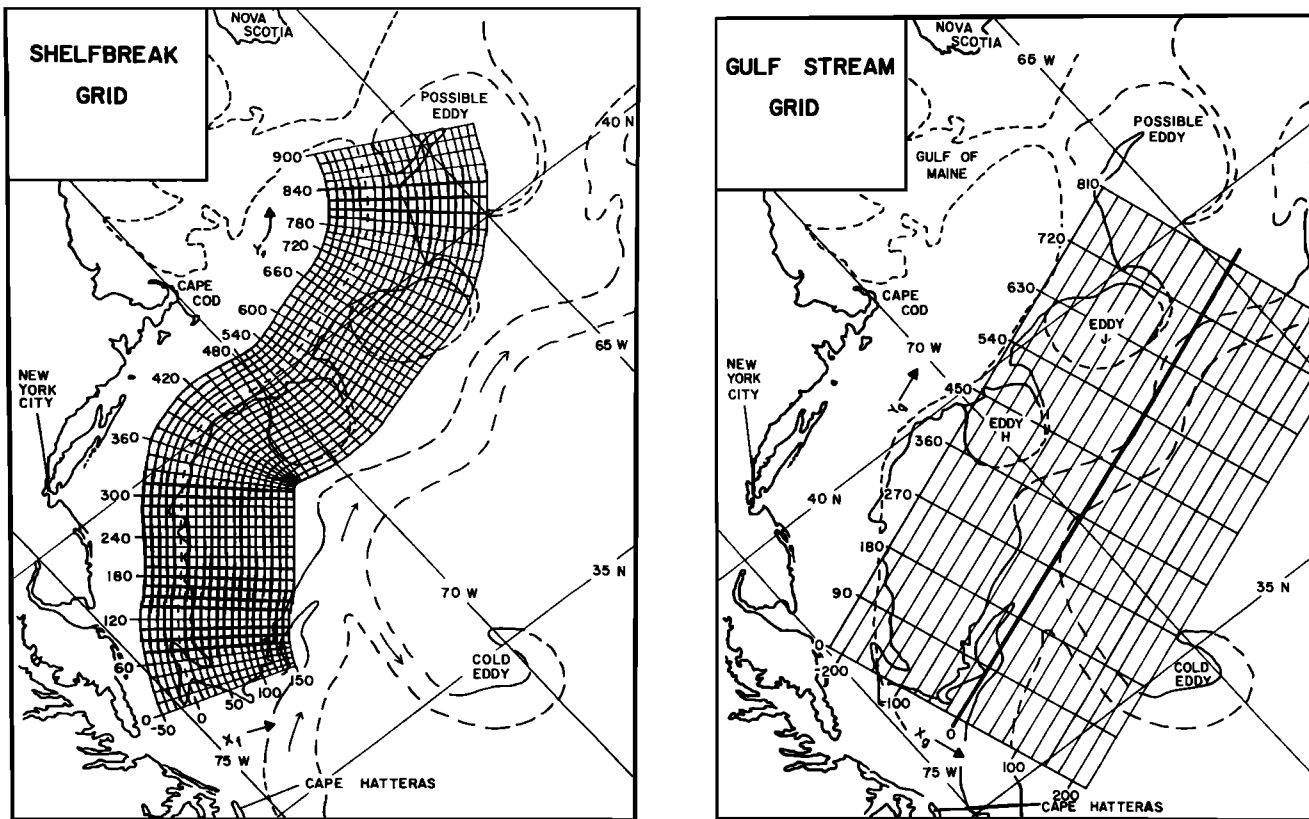


Fig. 1. The EOFFA chart of November 17, 1976, with the shelfbreak and Gulf Stream grids superimposed. The distance units are kilometers.

face front with spatial scales between 30 and 900 km and temporal scales between 2 weeks and 2 years.

*Gulf stream meanders and warm-core, anticyclonic eddies.* Downstream of Cape Hatteras, Hansen [1970] found meanders of the Gulf Stream with wavelengths between 200 and 400 km, which propagated downstream at 5–10 cm/s; the average wavelength was 320 km, and the average phase speed was 8 cm/s. Most meanders grew as they propagated downstream, which suggests that they were unstable. Robinson *et al.* [1974] studied the variability of the Gulf Stream with periods between 1 day and 2 months. Again, large-scale meanders grew and propagated downstream. In addition, meanders with periods as short as 1 day often produced cross-stream motions of the front several times greater than those associated with the large-scale meanders. Using Goes 1 images, Maul *et al.* [1978] found dominant periods of 45 and 5 days for Gulf Stream meanders off New England. The present study resolves the dominant, large-scale meanders but not those with periods less than 2 weeks.

The Gulf Stream meanders frequently grow large enough to produce cyclogenesis and anticyclogenesis. The anticyclonic eddies formed to the north of the Stream (for example, eddies H and J in Figure 1) are examined here for their influence on the shelf-slope front. Saunders [1971], Gotthardt [1973a], Gotthardt and Potocsky [1974], and Stumpf and Rao [1975] have studied their formation and 'life cycle' using satellite thermal imagery. They usually form east of 70°W. Those that form east of 65°W usually develop well offshore of the shelf-slope front, propagate westward to strike the Scotian Shelf or Georges Bank, and then propagate southwestward along the continental slope. Those that form between 65° and

70°W quickly make contact with the shelf-slope front. Most eddies are captured by the Gulf Stream as they approach Cape Hatteras, but some are captured earlier by large meanders of the Stream.

From 1970 through 1976 the average propagation speed for the eddies was 3.5–8 cm/s, and their life span was frequently greater than half a year [Lai and Richardson, 1977]. (In fact, eddy B was tracked for a year [Perchal, 1975].) Occasionally, eddies stall or drift slowly northeastward for short periods (2 or 3 weeks) before continuing southwestward. Twenty eddies were observed during the 7-year period, with an average of three present between Cape Hatteras and the Grand Banks. Their diameter averaged about 100 km, and they tended to shrink in size and propagate faster as they approached Cape Hatteras [Gotthardt, 1973b]. During 1974 and 1975 an average of three eddies per year affected Deepwater Dumpsite 106 (38.7°–39°N, 72°–72.5°W), where they had an average residence time of about 22 days per eddy [Bisagni, 1976].

Near the shelfbreak, the eddies tend to force near-surface shelf water offshore at their northeast edge (for example, eddies H and J in Figure 1), thereby forcing large-amplitude, seaward perturbations of the shelf-slope front. In one case, Morgan and Bishop [1977] observed a 50-m-thick 'tongue.' They estimated that a sizeable fraction of the total exchange across the shelf-slope front may result from the offshore entrainment of shelf water from these tongues. In another case, Saunders [1971] observed a 50-km-wide tongue; it extended from the surface to a depth of 170 m, the coldest water lying between 50 and 120 m. Hence the tongues of shelf water observed in satellite images cannot be dismissed arbitrarily as insignificantly thin.

Shoreward perturbations of the bottom front can be forced by the eddies in their southwest quadrant [Chamberlin, 1976]. However, shoreward movement of the surface front was not produced by most eddies examined in the present study.

#### METHODOLOGY

*The coordinate grids.* To digitize the weekly positions of the shelf-slope front, Gulf Stream front, and the eddies from the EOF charts, two coordinate systems were used. The shelfbreak grid (Figure 1), used to digitize the shelf-slope front and the eddies, is a curvilinear coordinate system aligned with the shelfbreak, represented by the 100-fathom (187-m) contour. This is a practical coordinate system for the shelf-slope front and the eddies because the mean position of the front is closely aligned with the shelfbreak, and the paths of the eddies are guided by the shelfbreak. The origin is located at the shelfbreak offshore of Cape Charles, Virginia, with  $x_f$  increasing offshore and  $y_f$  increasing to the northeast. The grid resolution is 10 km for  $x_f$ , which is about one half the internal radius of deformation near the shelfbreak, and 15 km for  $y_f$ . Owing to the curvature of the coordinate grid, the resolution of  $y_f$  is exactly 15 km only along the contour  $x_f = +30$  km, near the mean position of the surface front. The front and eddies were studied between Cape Charles and the Northeast Channel ( $0 \leq y_f \leq 900$  km), which separates Georges Bank from the Scotian Shelf. The front was not studied south of Cape Charles because it occasionally terminated there, as shown in Figure 1, owing to entrainment of shelf water by the Gulf Stream north of Cape Hatteras.

The Gulf Stream grid (Figure 1) is a Cartesian coordinate system approximately aligned with the mean position of the Stream's axis. The origin is located about 125 km northeast of Cape Hatteras. The cross-stream coordinate  $x_g$  is zero along the straight line on the EOF charts connecting ( $36^\circ\text{N}$ ,  $75^\circ\text{W}$ ) with ( $39^\circ\text{N}$ ,  $65^\circ\text{W}$ ) and increases seaward. The alongstream coordinate  $y_g$  increases to the northeast (downstream). The grid resolution is 25 km for  $x_g$ , which is about one half the internal radius of deformation near the Gulf Stream, and 90 km for  $y_g$ . The Stream was studied in the region  $0 \leq y_g \leq 810$  km. These end points are located approximately offshore of the end points of the shelfbreak grid.

*Digitization procedure.* Position data were digitized by overlaying the grids on the weekly EOF charts. The displacement,  $A_f(y_f, t)$ , of the shelf-slope front from the shelfbreak (the intersection of the front with  $x_f$ ) was digitized with a resolution of 5 km. Sixty-one time series, each 104 weeks long, were thus obtained. Occasionally, the frontal locus was multiple valued owing to the offshore entrainment of shelf water or the onshore entrainment of slope water. These consequent tongues, most of which were forced by the eddies, were usually deflected alongshore, describing a hook pattern. The minimum value of  $|A_f|$  was used in these cases.

The width (measured normal to the shelfbreak),  $A_e(y_f, t)$ , of the eddies was digitized using the shelfbreak grid. The domain and resolution for  $A_e$  were the same as those for  $A_f$ . A tongue of shelf water sometimes masked an eddy's northeast boundary. The middle of such an entrained tongue was taken to be the edge of the eddy.

The displacement,  $A_g(y_g, t)$ , of the Gulf Stream front from its approximate mean axis ( $x_g = 0$ ) was digitized with a resolution of 25 km. Ten time series, each 104 weeks long, were thus obtained. On five occasions, large meanders produced an S-shaped, multiple-valued frontal locus. In those cases the locus

was minimally smoothed to produce a single-valued position of the frontal locus, which was then digitized [Halliwell, 1978].

*Sampling errors.* Errors arise in the preparation of the EOF charts and in the digitization procedure. The EOF errors result primarily from poor satellite images, overlay misalignments, and distortions due to the earth's sphericity [Perchal, 1976]. In the images, fronts can be obscured by cloud cover or if their surface temperature gradients are weak. Off the northeast United States cloud cover is most prevalent in winter, owing to frequent storms and the offshore advection of cold air over warmer water. Weak surface temperature gradients are common during summer, owing to seasonal heating. If the horizontal temperature change is of the order of the difference ( $0.5^\circ\text{C}$ ) between the discrete temperature levels sensed by the NOAA satellites, a 'false front' may appear in the image. Different shades of grey are assigned to each  $0.5^\circ\text{C}$  temperature band; thus if the temperature of the surface water gradually increases seaward, such as  $0.6^\circ\text{C}$  in 30 km, a change in grey tone will appear on the image within that 30-km interval. Sometimes these false fronts can be rejected on the basis of pattern recognition, but they may occasionally follow the shelfbreak and be mistaken for the actual front.

As a consequence of the above factors, there is no best time of the year in which to track the fronts by satellite thermal imagery. Also, these images cannot routinely provide synoptic coverage of the fronts at precisely 1-week intervals. Usually, sections of a front must be located in two or more images during a week, and some sections may be obscured for the entire week. Sea surface temperature observations from ships and aircraft are used to help locate the fronts, but these observations are made irregularly in space and time and with low resolution except in the case of some research vessels. All available data are used to produce a 'best guess' of a representative frontal position for the week. Frontal boundaries are located within 5–10 km of their true positions when good images of strong surface temperature fronts and good sea truth data are available, (R. J. Perchal, personal communication, 1978) and within 20–40 km when they are not [Perchal, 1976]. When minimal cloud cover allows sighting a front, solid lines are drawn on the EOF charts; otherwise, dashed lines are drawn based on the previous chart. For any particular location in our domain, fronts can be accurately located about 75% of the time on a weekly basis. Examination of several time series of the shelf-slope and Gulf Stream fronts [Halliwell, 1978] did not reveal notable variations in frontal position between periods of good and poor data; changes in frontal position between these periods were less than the worst-case error estimates given above. Consequently, no distinction is made between periods of good and poor data in this study.

Quantization errors occur because  $A_f$ ,  $A_e$ , and  $A_g$  are estimated at discrete values. The rms value of the quantization error is [Bendat and Piersol, 1971]  $qe \approx 0.29\Delta A$ , where  $\Delta A$  is the resolution. Hence  $qe$  is about 1.5 km for  $A_f$  and  $A_e$  and about 7.5 km for  $A_g$ . For  $A_f$  and  $A_e$  the EOF errors are larger than the quantization errors; while for  $A_g$  they may be equal when good quality images of the Gulf Stream are available.

Computed alongshelf scales and phase speeds of the shelf-slope front perturbations and the eddies are affected by the mean displacement of the front from the shelfbreak due to the grid's curvilinearity. This is not a serious problem for the shelf-slope front because its space-time average displacement is near  $x_f = +30$  km, where the alongshelf scales are not affected. On average, the centers of the eddies were located at  $x_f$

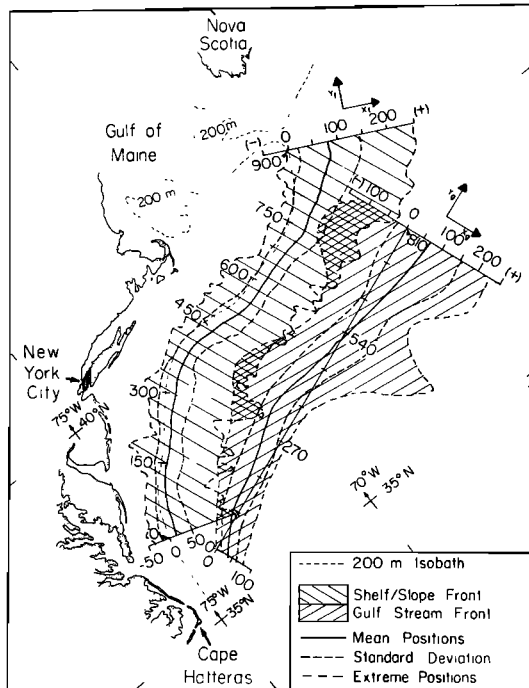


Fig. 2. Mean position, standard deviation envelope, and extreme positions of the shelf-slope and Gulf Stream surface temperature fronts for both-years (September 1975 through August 1977). The distance units are kilometers.

= +80 km. At this distance offshore the alongshelf resolution of  $y_j$  was not uniform; it ranged from 19 km south of Georges Bank to 8 km near Hudson Canyon. The total length of the  $x_j$  = +80 km contour is 860 km; thus the spatially averaged estimates of alongshelf scales and propagation speeds of the eddies are accurate to within several percent.

The amplitudes of the dominant perturbations of the shelf-slope and Gulf Stream fronts were an order of magnitude larger than the estimated errors on the EOF charts. Also, the time scales of the dominant perturbations were a month or more; hence there was signal processing gain in extracting their 'signatures' from the week-to-week noise in the EOF charts. Errors in locating the boundaries of the eddies were small in comparison with the average eddy diameter.

**Analyses performed.** The analyses of the displacement include basic statistics (mean position, standard deviation, and extreme positions (Figure 2 only)), empirical orthogonal functions (EOF's), autocorrelation functions (space, time, and space-time), autospectra (wave number, frequency, and wave-frequency), and wave number-frequency cross spectra. These analyses are discussed below. They were performed for the entire 2-year data set, hereafter referred to as the 'both-years' case. To detect interannual variability, most analyses were also performed separately for years one and two. The year one, year two, and both-years cases are referred to collectively as the 'three cases.' All statistical significance is measured at the 90% confidence level.

**Empirical orthogonal functions.** EOF's were computed for the shelf-slope and Gulf Stream fronts. They decompose the horizontal alongshelf (or alongstream) structure into several empirical modes representing spatially coherent structures, each with a time varying amplitude. Each EOF, or empirical mode, accounts for a fraction of the total variance (i.e., of the sum of the variances of all the time series) of the frontal dis-

placement, and most of the total variance is expected to be accounted for by a small fraction of the total number of modes. The modes are ordered according to the percent variance they account for, with mode one accounting for the most variance, and so forth. The most significant modes have a large signal-to-noise ratio, while the least significant modes are essentially pure noise. The structure and the temporal variability of the dominant perturbations are determined from the most significant modes. EOF's represent stationary spatial patterns. Propagating perturbations may be resolved into two or more EOF's of similar structure whose linear combination reproduces the propagating waves in the same manner that a propagating, periodic wave form can be represented by a linear combination of sine and cosine functions. EOF's of the eddies [Halliwell, 1978] are not discussed here because the size and speed of the eddies were adequately determined from the correlation and spectrum analyses. The basic computational procedure is outlined below and follows *Inspersen* [1971].

The  $A(y_i, t)$  are discrete time series samples at points  $y_i$ ,  $i = 1, 2, \dots, M$ . These series represent the amplitudes ( $A_f$  or  $A_g$ ) of the shelf-slope or Gulf Stream fronts. The components of the covariance matrix of these time series are

$$R_{ij} = \langle A(y_i, t)A(y_j, t) \rangle$$

where the angle brackets denote time average. The  $M$  eigenvectors and eigenvalues of this matrix are found by solving

$$(\tilde{R} + \lambda_k)\phi_k(y_i) = 0$$

$$k = 1, 2, \dots, M \quad l = 1, 2, \dots, M$$

where the  $\lambda_k$  are the eigenvalues of the covariance matrix  $\tilde{R}$ . The eigenvectors define a set of orthogonal functions such that

$$\sum_{i=1}^M \phi_k(y_i)\phi_m(y_i) = \delta_{km}$$

where  $\delta_{km}$  is the Kronecker delta. The original time series are expanded in terms of the eigenvectors to compute the modal amplitude time series

$$b_k(t) = \sum_{i=1}^M \phi_k(y_i)A(y_i, t) \quad k = 1, 2, \dots, M$$

where  $\langle b_k(t)b_m(t) \rangle = \lambda_k \delta_{km}$  and  $\lambda_k$  is the  $k$ th eigenvalue. The original time series are represented in terms of the EOF's as follows:

$$A(y_i, t) = \sum_{k=1}^M b_k(t)\phi_k(y_i)$$

The eigenvectors, the  $\phi_k(y_i)$  represent the EOF's of  $A$ , while the  $b_k(t)$  are their time varying amplitudes. The variance associated with each  $\phi_k$  equals  $\lambda_k$ . The fraction of the total variance accounted for by each EOF is

$$\alpha_k = \lambda_k / \left( \sum_{i=1}^M \lambda_i \right) \quad k = 1, 2, \dots, M$$

The efficiency with which EOF's account for the variance is given by their entropy  $H$  [cf. *O'Neill*, 1963]:

$$H = - \sum_{k=1}^M \alpha_k \ln \alpha_k$$

If all of the variance resides in one mode (perfect order),  $H = 0$ ; if the variance is evenly distributed among all modes

(perfect disorder),  $H = \ln(M)$ . The normalized entropy,  $H' = H/\ln(M)$ , is used to compare the entropies of different systems having different  $M$ , such as the Gulf Stream and shelf-slope fronts in this study.

**Correlation functions.** The temporal and spatial autocorrelation functions for  $A(y_i, t_j)$ ,  $i = 0, 1, 2, \dots, M$ ;  $j = 0, 1, 2, \dots, N$ , with  $A$  demeaned and uniform sampling intervals  $\Delta y$  and  $\Delta t$ , are

$$R_{im}(y_i, \tau_m) = \frac{1}{C(y_i, 0)(N - m)} \sum_{j=0}^{N-m} A(y_i, t_j)A(y_i, t_j + \tau_m)$$

and

$$R_{il}(\xi_i, t_i) = \frac{1}{C(0, t_i)(M - l)} \sum_{j=0}^{M-l} A(y_j, t_j)A(y_j + \xi_i, t_j + t_i)$$

where  $\tau_m = m\Delta t$  is the lag time,  $\xi_i = l\Delta y$  is the lag distance, and  $C(y_i, 0)$  and  $C(0, t_i)$  are the autocovariance functions at zero lag time and lag distance, respectively. Thus the temporal and spatial autocorrelation functions are normalized to equal 1 at zero lag time and zero lag distance, respectively.

The space-time autocorrelation function is

$$R_{im}(\xi_i, \tau_m) = \frac{1}{(M - l)(N - m)} \sum_{j=0}^{M-l} \frac{1}{C(y_j, 0)} \cdot \sum_{k=0}^{N-m} A(y_j, t_k)A(y_j + \xi_i, t_k + \tau_m)$$

which is normalized to equal 1 at zero lag time and zero lag distance. If a dominant perturbation propagates with a speed  $c$ , a ridge of relatively high correlation occurs at values of  $\xi$  and  $\tau$  such that  $c = (d\xi/d\tau)$ . This criterion is used to estimate propagation speeds for perturbations of the shelf-slope and Gulf Stream fronts and of eddies moving along the shelf-break.

Temporal or spatial correlation scales are estimated as the lag time or lag distance at which the corresponding autocorrelation functions decrease below a certain value. This value is chosen by employing the technique for cross-correlation functions outlined by Davis [1976], and here it approximately equals 0.3 at a 90% level of confidence.

**Spectrum functions.** Frequency,  $\sigma$ , autospectra were computed by Fourier transforming the temporal autocovariance functions and averaging over the spatial domain. These autocovariance functions were computed from time series normalized by their individual standard deviations for both-years. Thus changes in the frequency spectrum of  $A_f$ ,  $A_e$ , and  $A_g$  between years one and two could be studied. (Normalization was performed to prevent the larger variance of the shelf-slope and Gulf Stream fronts in the northeastern part of their domains from dominating the spectra.) Wave number,  $k$ , autospectra were computed by Fourier transforming the spatial autocovariance functions over the time domain. These autocovariance functions were computed from space series normalized by the overall, i.e., for the entire spatial domain and both-years, standard deviation. Thus changes in the wave number spectrum of  $A_f$ ,  $A_e$ , and  $A_g$  between years one and two could be studied.

Wave number-frequency autospectra were computed using methods outlined in the work of Pratt [1976], with one major change: the spectrum estimates were computed for positive frequency versus both positive and negative wave number instead of positive wave number versus both positive and nega-

tive frequency. Time series normalized over the 2-year period were used. The space-time demeaned series  $A(y_j, t_i)$ ,  $j = 0, 1, 2, \dots, M$ , and  $i = 0, 1, 2, \dots, N$ , were expanded into temporal Fourier harmonics as follows:

$$A(y_j, t_i) = \sum_{n=1}^N [C_n(y_j) \cos(\sigma_n t_i) + S_n(y_j) \sin(\sigma_n t_i)]$$

The wave number autospectra and cross spectra of the functions  $C_n(y_j)$  and  $S_n(y_j)$  for frequency  $\sigma_n$  and wave number  $k_n$  are given by  $W_m(C_n)$ ,  $W_m(S_n)$ ,  $K_m(C_n, S_n)$ , and  $Q_m(C_n, S_n)$ , where  $W_m$  is the wave number autospectrum for  $C_m$  or  $S_m$ , and  $K_m$  and  $Q_m$  are the wave number cospectrum and quadrature spectrum for  $C_n$  and  $S_n$ , respectively. (These spectra were smoothed by Hanning.) The ordinary wave number-frequency autospectrum is

$$E(\pm k_m, \sigma_n) = \frac{1}{2}[W_m(C_n) + W_m(S_n)] \pm \frac{1}{2}Q_m(C_n, S_n)$$

The total wave number-frequency autospectrum, i.e., without regard for the sign of  $k$ , is

$$T(k_m, \sigma_n) = E(+k_m, \sigma_n) + E(-k_m, \sigma_n) = \frac{1}{2}[W_m(C_n) + W_m(S_n)]$$

The contribution from propagating waves is the difference between  $E(+k_m, \sigma_n)$  and  $E(-k_m, \sigma_n)$ , viz.,  $PR(k_m, \sigma_n) = Q_m(C_n, S_n)$ , which is called the propagating wave number-frequency autospectrum. (Pratt [1976] defined  $PR$  to be the absolute value of this quantity.) If  $PR > 0$ , the waves propagate toward positive  $y$ . The contribution from standing waves is

$$ST(k_m, \sigma_n) = K_m^2(C_n, S_n) + \frac{1}{4}[W_m(C_n) - W_m(S_n)]^2$$

which is independent of standing wave phase and is called the standing wave number-frequency autospectrum. The phase of the antinode of the standing waves is

$$\Phi(k_m, \sigma_n) = \tan^{-1} \frac{2K_m(C_n, S_n)}{W_m(C_n) - W_m(S_n)}$$

If the coherence squared between  $C_n$  and  $S_n$  equals 1, all the nonpropagating variance is due to standing waves; if it is small, the nonpropagating variance is primarily random noise. Thus a significant fraction of the total variance at each wave number and frequency was judged to result from standing waves when this coherence was significant. Clearly, caution should be exercised in interpretation because the propagating and standing wave spectra may be correlated [Pratt, 1976].

The wave number-frequency cross spectrum between  $A_1(y, t)$  and  $A_2(y, t)$  is

$$E_{12}(\pm k_m, \sigma_n) = \frac{1}{2}K_m(C_{1m}, C_{2n}) + K_m(S_{1m}, S_{2n}) \pm \frac{1}{2}[Q_m(C_{1m}, S_{2n}) + Q_m(C_{2m}, S_{1n})]$$

where  $C_{1n}(y_j)$ ,  $S_{1n}(y_j)$ ,  $C_{2n}(y_j)$ , and  $S_{2n}(y_j)$  are the temporal Fourier coefficients of  $A_1$  and  $A_2$ . The wave number-frequency coherence squared between  $A_1$  and  $A_2$  is

$$\gamma_{12}^2(\pm k_m, \sigma_n) = \frac{E_{12}^2(\pm k_m, \sigma_n)}{E_1(\pm k_m, \sigma_n)E_2(\pm k_m, \sigma_n)}$$

where  $E_1$  and  $E_2$  are the ordinary wave number-frequency autospectra.

The wave number, frequency, and total wave number-frequency autospectra were multiplied by  $k$ ,  $\sigma$ , and  $k$  times  $\sigma$ , respectively, to enhance their spectral peaks. Before computing their wave number-frequency cross spectrum, 'denoised' time series were constructed for  $A_f$  and  $A_g$  using only the first five

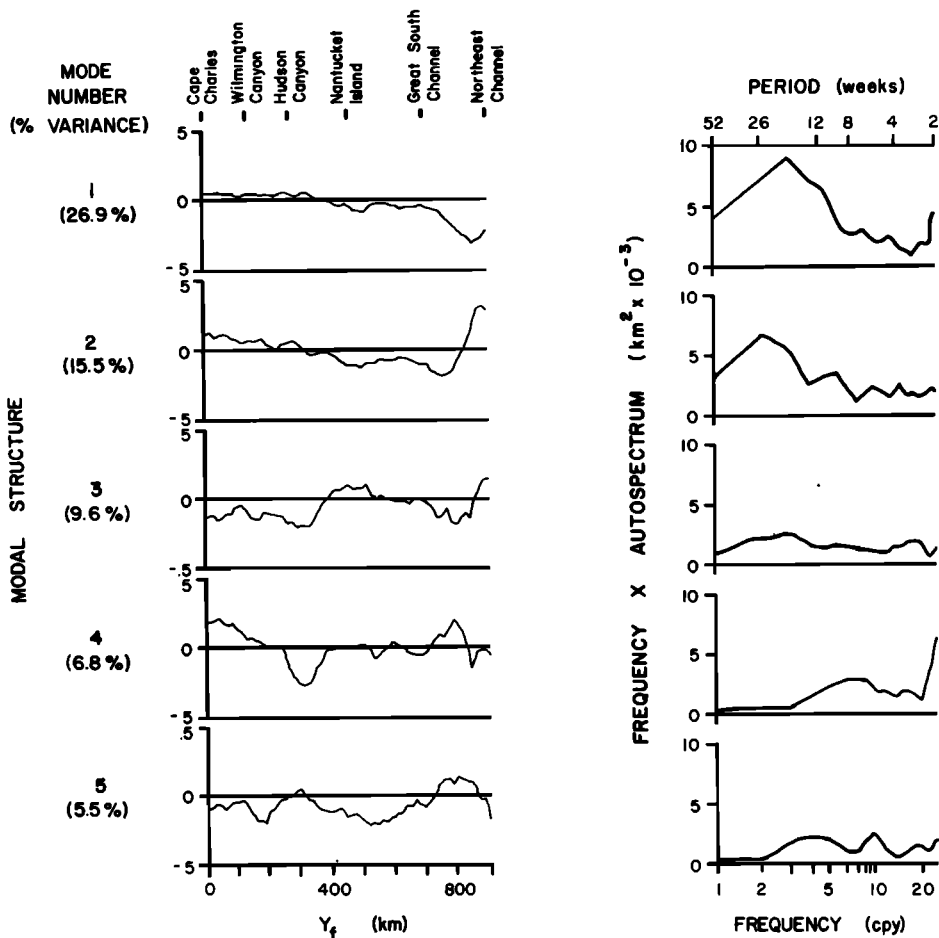


Fig. 3. Shelf-slope front. The five most significant EOF modes (modal structures and autospectra of the EOF amplitudes) for both-years.

EOF's. The wave number–frequency spectra were band averaged uniformly over six adjacent bands.

SHELF-SLOPE FRONT

*Notable features.* Based on space-time contours of  $A_f$  [Halliwell, 1978], large seaward displacements of the front

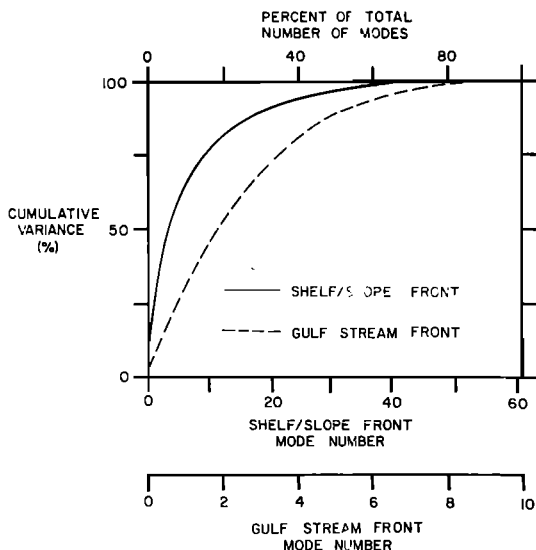


Fig. 4. Cumulative variance as a function of EOF mode number for the shelf-slope and Gulf Stream fronts (both-years).

were frequent along eastern Georges Bank (and northeastward along the southern Scotian Shelf). They were usually associated with the presence of eddies, and they often persisted for several weeks. Between Cape Charles and the Great South Channel, the front was more tightly bound to the shelf-break except during the passage of vigorous eddies, which forced large, seaward perturbations of the surface front at their northeastern edge. These perturbations had alongshelf scales of about 100 km. The eddies did not force large shoreward perturbations of the surface front at their southwestern edge. Twice as many eddies interacted with the front during year two than during year one, as is discussed in the next section. Also, the eddies forced larger and more frequent seaward perturbations southwest of Georges Bank during year two. Hence there were substantial interannual variations in the frequency and intensity of these eddies (at least those detectable in IR imagery) and in the response of the shelf-slope front to their passage.

The front moved shoreward of the shelfbreak for three exceptionally persistent episodes. For the first episode (south-

TABLE 1. Normalized Entropy for the Shelf-Slope and Gulf Stream Fronts

	Shelf-Slope Front	Gulf Stream Front
Year 1	0.56	0.74
Year 2	0.66	0.74
Both-years	0.63	0.78

TABLE 2. Correlation Scales From the Spatial and Temporal Autocorrelation Functions

	Shelf-Slope Front		Eddies		Gulf Stream Front	
	Spatial	Temporal	Spatial	Temporal	Spatial	Temporal
Year 1	80 ± 53	1.9 ± 1.5	80 ± 15	1.9 ± 1.1	97 ± 45	2.8 ± 1.7
Year 2	67 ± 38	2.5 ± 1.1	81 ± 18	2.6 ± 1.0	87 ± 35	2.3 ± 0.9
Both-years	74 ± 46	2.2 ± 1.1	81 ± 18	2.3 ± 1.2	92 ± 42	2.5 ± 1.1

Spatial scales are in kilometers, and temporal scales are in weeks.

west of Georges Bank ( $600 < y_f < 850$  km) between weeks 2 and 16), no forcing mechanisms were apparent in the EOF charts. (Upstream influences, e.g., from the Labrador Current, could be responsible, but they can only be speculated on here.) For the second episode (along the New England shelf and western Georges Bank ( $450 < y_f < 800$  km) between weeks 50 and 60) a large northward meander of the Gulf Stream (which became eddy H by week 54) moved close to the shelfbreak south of Georges Bank during week 50 and may have forced the surface front shoreward. (In the next section the 'uncovering' of an eddy off the Middle Atlantic Shelf by Hurricane Belle during week 51 is discussed.) For the third

episode (south of the New York Bight ( $y_f < 300$  km) between weeks 66 and 83) the Gulf Stream shifted up to 60 km shoreward southeast of the Middle Atlantic Shelf. Hence based on the second and third episodes, the Gulf Stream itself apparently perturbs the shelf-slope front on some occasions.

Frequently, perturbations of the front were not obviously forced by the eddies or the Stream. These perturbations had typical alongfront scales of less than 80 km and cross-front amplitudes of less than 50 km. (Voorhis *et al.* [1976], Beardsley and Flagg [1976], and Flagg [1977] documented similar perturbations.) They usually could not be located on consecutive EOF charts; hence a sampling interval shorter than the 1 week is required to resolve them.

*Statistics of  $A_f$ .* For both years the mean and standard deviation of the displacement of the front from the shelfbreak averaged about  $+20 \pm 30$  km (Figure 2) between Cape Charles and the Great South Channel and then increased to about  $+80 \pm 65$  km near the Northeast Channel, consistent with the statistics of Ingham [1976] and Gunn [1979]. The domains of the shelf-slope and Gulf Stream fronts overlapped; occasionally, these fronts were in direct contact. The rms amplitude doubled from year one to year two between Cape Charles and the Great South Channel, probably owing to the stronger influence of eddies. In contrast, the rms amplitude decreased substantially from year one to year two near the Northeast Channel, which was indicative of less vigorous forcing by eddies in that subdomain.

*Empirical orthogonal functions.* The first five modes accounted for about two-thirds of the total variance during both-years (Figure 3). Ninety-five percent of the total variance was accounted for by the first 26 modes (Figure 4). The normalized entropy was 0.63 (Table 1).

Mode one had a relatively large amplitude along Georges Bank (Figure 3). The maximum amplitude occurred near Northeast Channel, and most of the variance was concentrated between 1 and 6 cpy (cycles per year). The time varying amplitude of mode one (not shown) was large when the eddies south of eastern Georges Bank perturbed the front. One of mode two's nodal points was near  $y_f = 830$  km; hence some of the perturbations between Hudson Canyon and the center of Georges Bank were  $180^\circ$  out of phase with those at the eastern end of the Bank. Modes one, two, and three had nodal points south of Long Island; hence these perturbations tended to be  $180^\circ$  out of phase between the Middle Atlantic and New England Shelves. Mode four was relatively large near Cape Charles and Hudson Canyon and along Georges Bank; each of these maxima had an alongshelf scale of about 100 km. The time varying amplitude of mode four (not shown) was very large when the eddies perturbed the front near Hudson Canyon. Mode five was in phase throughout the Middle Atlantic Bight except between a pair of nodes near Hudson Canyon.

The structure of the perturbations changed from year one to year two. For years one and two, mode one was similar, but that of year two had a smaller amplitude along Georges Bank

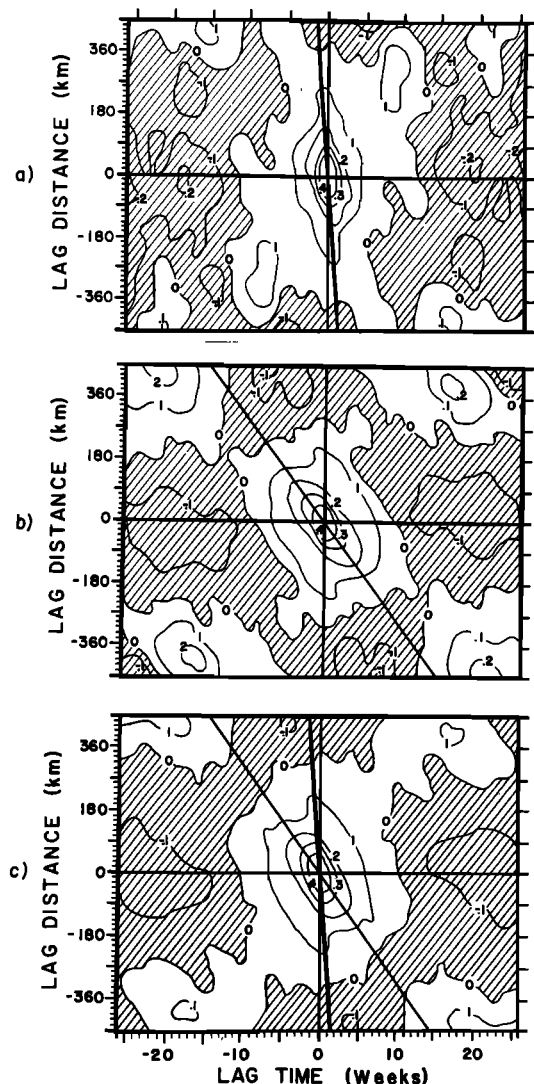


Fig. 5. Shelf-slope front. Space-time autocorrelation functions of normalized  $A_f$  for (a) year one, (b) year two, and (c) both-years. The average propagation speeds equal the slopes of the dark lines (see Table 2).

TABLE 3. Correlation Scales and Propagation Speeds From the Space-Time Autocorrelation Functions

	Shelf-Slope Front			Eddies			Gulf Stream Front		
	Spatial	Temporal	Speed	Spatial	Temporal	Speed	Spatial	Temporal	Speed
Year 1	90	1.8	-40	70	1.8	-8	100	2.7	+6
Year 2	65	2.5	-5	65	2.5	-5	85	2.3	+7
Both-years	80	2.2	-40, -5	70	2.2	-6	90	2.5	+7

Spatial scales are in kilometers, temporal scales in weeks, and propagation speeds in centimeters per second. Space-time autocorrelation functions are from Figures 5, 11, and 17. Negative speeds correspond to southwestward propagation.

[Halliwell, 1978]. Mode one accounted for 39% of the total variance during year one but only 20% during year two. In the three cases, mode two was virtually identical. Few similarities were noted between years among modes three and greater. The normalized entropy for years one and two was 0.56 and 0.66, respectively. The greater disorder during year two may have been due to the stronger influence of the eddies.

**Correlation analyses.** The spatial and temporal correlation scales for  $A_f$  are summarized in Table 2. (The  $A_f$  series were normalized before computing these functions to prevent the low-frequency, large-amplitude variability near Georges Bank from dominating the results.) The spatial correlation scale decreased from a mean of 80 to 67 km from year one to year two, and its standard deviation decreased from 53 to 38 km, probably indicative of the increased influence of the eddies. The mean spatial correlation scale was  $74 \pm 46$  km for both-years and occasionally as small as 25 km during weeks when the front was mainly perturbed by small-scale features. Thus to spatially resolve these features at all times, an alongshelf sampling rate of about 25 km is required.

The mean temporal correlation scale was significantly greater during year two (2.5 versus 1.9 weeks). For both-years it averaged  $2.2 \pm 1.1$  weeks between Cape Charles and the

Northeast Channel; it was about 4 weeks along Georges Bank and 1–3 weeks along the Middle Atlantic Shelf. Thus to resolve much of the variability at all locations along the front, a temporal sampling rate of about 1 week is required. (To fully resolve the response of the front to atmospheric storms, which have time scales between 2 and 10 days, a daily sampling rate is required. The sampling rates discussed above are adequate for studying the response of the front to offshore forcing and long-period (>2 week) variability in atmospheric forcing, which includes the integrated response to storms.)

The correlation scales and propagation speeds computed from the space-time autocorrelation function (Figure 5) are summarized in Table 3. These scales were similar to those estimated from the spatial and temporal autocorrelation functions. During year one the average southwestward propagation speed (40 cm/s) was consistent with that of coastally trapped waves [Wang and Mooers, 1976]. During year two the average southwestward propagation speed (5 cm/s) approximated that of the eddies, as is discussed in the next section. For both-years the propagation speeds of 40 and 5 cm/s were dominant. In the three cases (Figure 5) there were four secondary correlation maxima near lag distances of  $\pm 450$  km and lag times of  $\pm 20$  weeks. They were probably due to standing perturbations with average wavelength and period equal to those lag scales.

**Spectrum analyses.** The frequency autospectra for the three cases (Figure 6a) did not have any large peaks. The amplitude of the autospectrum function was greater during year two at most periods, with the largest increase (up to 45%) in the period band 13–52 weeks, and a smaller increase in the band 6–9 weeks. The autospectra decreased roughly as  $\sigma^{-1}$  for the three cases. (The spectra in Figure 6a are roughly 'white,' since they were multiplied by frequency.) The average spectrum estimate at a period of 2 weeks for unnormalized time series for both-years was  $53 \text{ km}^2/\text{cpy}$ , a value which is an order of magnitude greater than the quantization error ( $2.5 \text{ km}^2/\text{cpy}$ ), probably owing to aliasing.

The wave number autospectra for the three cases (Figure 6b) increased in amplitude by about 50% for wavelengths greater than 200 km and by about 25% for wavelengths less than 200 km from year one to year two. The wave number autospectra of displacement decreased as  $k^{-1}$  for  $k < 5 \times 10^{-3}$  cpk (cycles per kilometer) and as  $k^{-2}$  for  $k > 5 \times 10^{-3}$  cpk. There was a peak at a wavelength of 225 km in year two, which may have been associated with the seaward perturbations forced by the eddies. The alongshelf dimension of these perturbations was typically about 100 km, and they were separated by about 200 km, or greater, which is consistent with this spectral peak.

The ordinary wave number–frequency autospectrum for both-years (Figure 7a) had a maximum ridge at 'negative' wave numbers, indicating the dominance of southwestward propagating perturbations. The most energetic perturbations

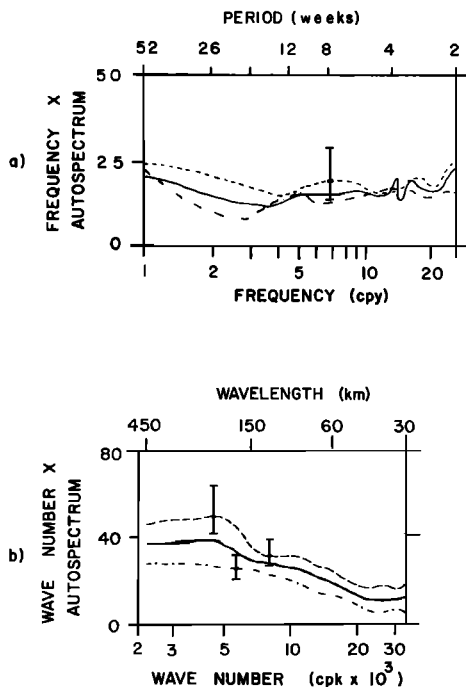


Fig. 6. Shelf-slope front. (a) Frequency autospectra (multiplied by  $\sigma$  to enhance the peaks) of normalized  $A_f$ , computed with 44 degrees of freedom. (b) Wave number autospectra (multiplied by  $k$  to enhance the peaks) of normalized  $A_f$ , computed with 200 degrees of freedom. Year one is shown by the dash-dot curve, year two by the dashed curve, and both-years by the solid curve.

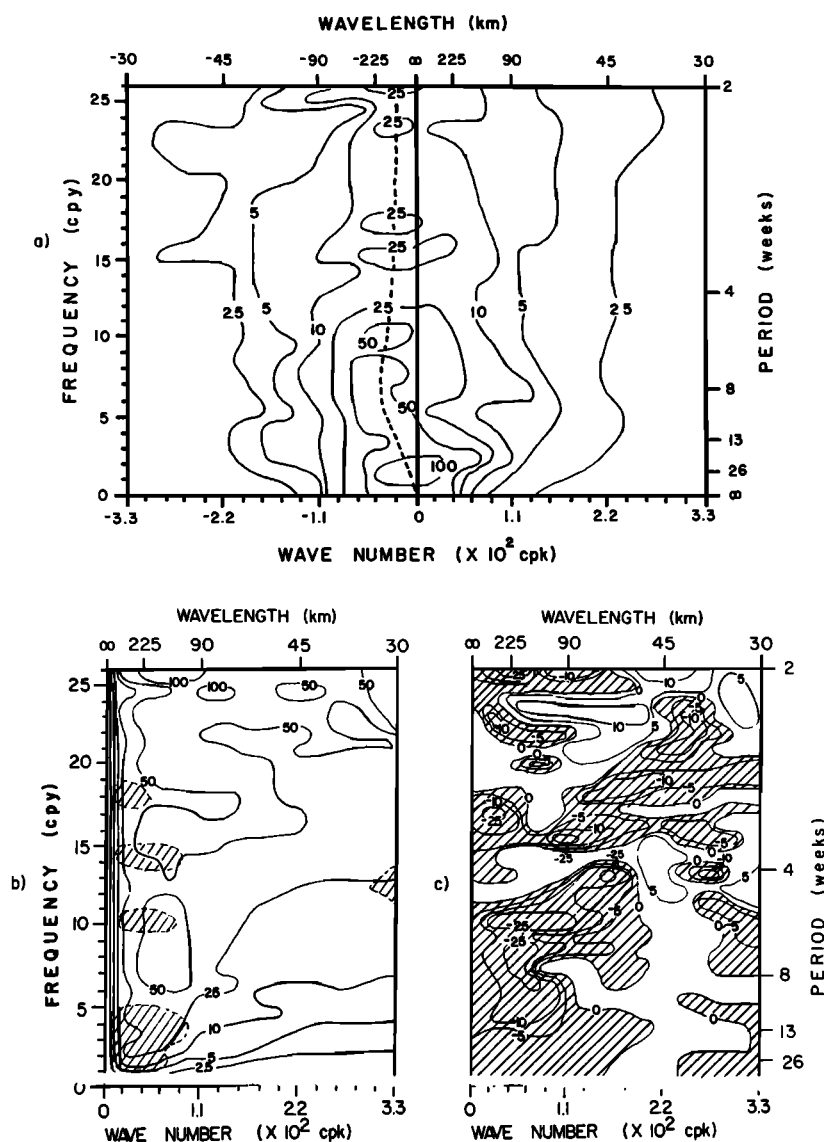


Fig. 7. Shelf-slope front. The wave number–frequency autospectra for both-years, computed with 12 degrees of freedom. (a) The ordinary autospectrum, where the dashed line denotes a maximum ridge. (b) The total autospectrum times  $10^4$  (multiplied by  $k$  and  $\sigma$  to enhance the peaks), where the shading shows those regions in  $(k, \sigma)$  space in which a significant fraction of the total variance is due to standing waves. (c) The propagating wave autospectrum, where shading indicates propagation toward negative  $y_r$ .

had wavelengths greater than 100 km and periods greater than 4 weeks. The total wave number–frequency autospectrum (Figure 7b) for both-years had significant peaks with wavelength and period bands summarized in Table 4. (The autospectra for the years one and two are shown in the work of Halliwell [1978].) The dominant perturbations had wavelengths of 100–300 km and periods of about 4–20 weeks, with

little change between years one and two. A spectral peak occurred during year one and both-years with wavelengths between 70 and 220 km and a period of about 2 weeks.

The standing wave number–frequency autospectrum for both-years was dominated by motions with wavelengths between 100 and 500 km and periods between 10 and 52 weeks. From an analysis of standing-wave phase a node for a long-

TABLE 4. Predominant Wavelength-Period Bands of the Wave Number–Frequency Total Autospectra

	Shelf-Slope Front		Eddies		Gulf Stream Front	
	$\lambda$ , km	$T$ , weeks	$\lambda$ , km	$T$ , weeks	$\lambda$ , km	$T$ , weeks
Year 1	100–300	3.5–20	90–300	2.5–17	220–900	7.4–17
	70–220	2.0–2.1				
Year 2	100–300	4.3–20	90–300	2.5–17	180–900	7–17
					180–450	2.7–3.3
Both-years	100–300	4.3–20	90–300	2.5–26	180–900	7.0–26
	70–220	2.0–2.1			180–450	2.7–3.3

Both-years cases are based on Figures 7, 13, and 19.

TABLE 5. Predominant Wavelength Period Bands and Associated Propagation Speeds of the Wave Number-Frequency Propagating Autospectra

	Shelf-Slope Front			Eddies			Gulf Stream Front		
	$\lambda$ , km	$T$ , weeks	Speed, cm/s	$\lambda$ , km	$T$ , weeks	Speed, cm/s	$\lambda$ , km	$T$ , weeks	Speed, cm/s
Year 1	90-300	3.5-10	-2 to -14	90-300	2.5-17	-1 to -20	220-600	5.8-17	2-17
	90-600	2.0-2.3	-7 to -50						
Year 2	90-300	4.3-17	-1 to -11	90-300	3.1-17	-1 to -16	220-600	7.4-17	2-13
Both-years	90-300	4.3-13	-3 to -11	90-300	2.5-26	-1 to -20	220-600	17-52	1-6
	70-600	2.0-2.1	-6 to -50				220-600	5.8-10	3-17

Both-years cases are based on Figures 7, 13, and 19. Negative speeds correspond to southwestward propagation.

period (13-26 weeks) standing wave with a wavelength of 450 km was located near Hudson Canyon, consistent with the EOF analysis and the space-time autocorrelation functions. The nodes for 450-km-wavelength standing waves with 3- to 5-week periods were also located near Hudson Canyon.

The propagating wave number-frequency autospectrum for both-years (Figure 7c) was dominated by motions with wavelengths of 90-300 km, periods of 4-13 weeks, and southwestward propagation speeds of 3-11 cm/s during both-years (Table 5). The scales and propagation speeds were similar for years one and two, but the dominant period band included some longer-period waves during year two. The average propagation speed of the dominant perturbations decreased during year two, as did the average propagation speed of the eddies (Table 3). Since the amplitude of this spectrum was about 30% larger during year two, the dominant perturbations were probably forced by the propagating eddies. There was a secondary maximum near a period of 2 weeks for southwestward propagating waves during year one and both-years (Table 5). For both-years the wavelength band was between 70 and 600 km, and the propagation speed ranged between 7 and 50 cm/s. Similar scales occurred for year one. The faster of these propagating perturbations may correspond to those noted in Table 3.

### EDDIES

**Notable features.** The alongshelf position,  $y_e$ , of the center of each of the 14 eddies observed during both-years provides a picture of their 'life history,' frequency of occurrence, and propagation speed (Figure 8). Twelve eddies are labeled with their letter names from the EOF charts; two were unnamed. (The letter names seemingly missing from Figure 8 had been assigned to eddies formed to the east of our domain and which never entered it.) Eight eddies formed near or to the east of Northeast Channel, including B and C before the start of this study, and propagated into our domain. Most of them

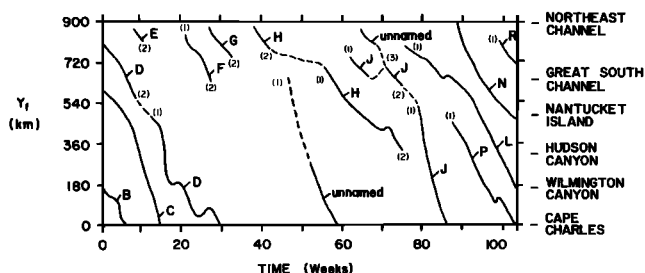


Fig. 8. Location of eddy centers as a function of  $y_e$  and time. Numeral (1) signifies formation (or reformation) of an eddy, numeral (2) signifies capture of an eddy by the Gulf Stream, and numeral (3) signifies the coalescence of two eddies.

formed to the east-southeast of Northeast Channel, then propagated westward until they collided with the shelfbreak west of Northeast Channel ( $y_f < 900$  km). Four eddies formed south of Georges Bank and one south of New England. Four of these five formed during year two. The Gulf Stream tended to shed eddies farther upstream during year two; in other words, the meanders may have grown faster downstream from Cape Hatteras during year two than during year one.

The evolution of the surface manifestation of an eddy first detected offshore of New Jersey at week 51 (August 18, 1976) is illustrated in a sequence of positions of the shelf-slope and Gulf Stream fronts for weeks 50-54 (Figure 9). At week 50, no unusual perturbations were observed along the shelf-slope front, and the Gulf Stream was about 200 km offshore. By week 51 a tongue of near-surface shelf water extended offshore near Hudson Canyon, forming an anticyclonic hook pattern. By week 52 a well-defined (but unnamed) eddy was visible. By week 53 a broad (about 100 km) tongue of shelf water had been driven offshore north of the eddy, while the Gulf Stream remained far offshore. The weak surface temperature gradients of late summer may have obscured the eddy until Hurricane Belle moved through its vicinity on August 10, the day prior to the EOF chart for week 50, producing enough mixing or near-surface advection to distinguish the eddy from its environs. On August 1 and 2 (during week 49) the eddy was apparent in an XBT (expendable bathythermograph) transect (obtained from the Naval Oceanographic Data Center) (NODC) off New Jersey. On September 1 and 2 (during week 53) a salinity maximum ( $>35\%$ ) was present in a surface salinity transect (obtained from NODC) through the center of the eddy; it was greater than the salinity of the surrounding slope water. Thus the eddy probably existed prior to its appearance on the EOF charts and was apparently shed by the Gulf Stream. The eddy may have formed from a large meander south of Georges Bank shown on the EOF chart of week 42 (June 16); this meander was missing from the chart of week 43. From the charts of weeks 43 and 44, there was a large area of mixed Gulf Stream and slope water south of Great South Channel. This thermal anomaly was irregular in shape, about 120 km normal and 200 km parallel to the shelf, and it was not present in the chart of week 45. If this anomalous feature was the eddy which appeared off New Jersey in early August, it traveled at 8 cm/s, which equals the average speed of eddies for both-years. The trace of this eddy, assuming that it formed near Great South Channel about week 43, is shown in Figure 8 as a dashed curve. Thus a consistent life history has been reconstructed for the eddy. We have no estimate of how often such eddies may remain 'undercover' in summer.

All eddies were eventually captured by the Gulf Stream. Four eddies were permanently captured by Gulf Stream

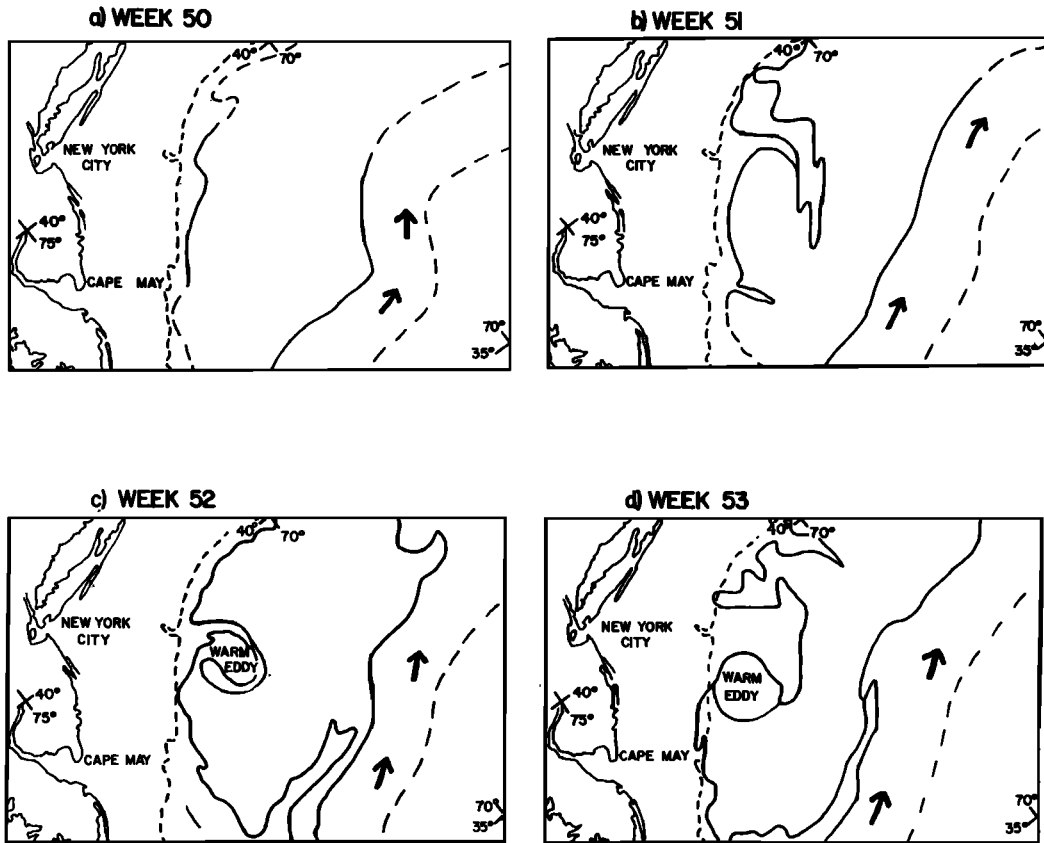


Fig. 9. Development of an eddy off New Jersey, based on EOF charts. (Week 50 corresponds to the chart dated August 11, 1976.)

meanders before reaching the Middle Atlantic Shelf, three south of Georges Bank and one south of New England (Figure 8). Two eddies coalesced south of Georges Bank at week 70. Eight eddies (including L and N after the end of this study) completed their journey to Cape Hatteras. Three eddies (D, H, and J) were temporarily captured by Gulf Stream meanders and subsequently released. D and J were captured

for about 3 or 4 weeks; H was captured for about 12 weeks by a standing meander. The life spans of the eddies ranged from 4 to 52 weeks. (The longest lived eddy, B, was discerned from formation to capture at Cape Hatteras for an entire year (October 31, 1974, to October 29, 1975 [Perchal, 1975, also personal communications, 1978].)

On the basis of Figure 8 and inspection of the EOF charts, the two years are divided into three periods: (1) during weeks 1–30, many eddies were observed, but they did not force notably large perturbations of the shelf-slope front; (2) during weeks 31–52, only one short-lived eddy (H prior to temporary capture) was observed; and (3) during weeks 53–104, numerous eddies were observed, and they forced large perturbations of the shelf-slope front. The propagation speed varied both from eddy to eddy and from week to week for each eddy, ranging generally between 2 and 15 cm/s to the southwest. Occasionally, an eddy briefly stalled or propagated toward the northeast.

*Statistics of  $A_e$ .* The number of eddies as a function of  $y_f$  for both-years was computed every 90 km within  $0 \leq y_f \leq 900$  km (Figure 10a). The southcentral portion of Georges Bank was impacted by more eddies (10) than any other region. The number of eddies contacting Georges Bank decreased to the east because the eddies tended to strike the shelf west of Northeast Channel. The number decreased to the west because four eddies were captured by Gulf Stream meanders, and two eddies coalesced within the interval  $450 \leq y_f \leq 720$  km. The mean maximum  $A_e$  for all eddies as a function of  $y_f$  (Figure 10b) decreased southwestward of Hudson Canyon ( $y_f = 300$  km). This decrease, from about 120 km for  $y_f \geq 360$  km to 90 km for  $y_f < 200$  km, suggests that the eddies were sub-

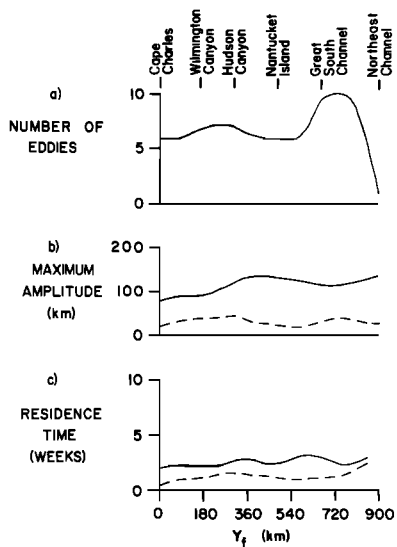


Fig. 10. Eddies. Statistics along the shelf for both-years: (a) the total number of eddies, (b) the maximum amplitude  $A_e$  of all eddies, and (c) the eddy residence time. The solid curve shows the mean, and the dashed curve shows the standard deviation.

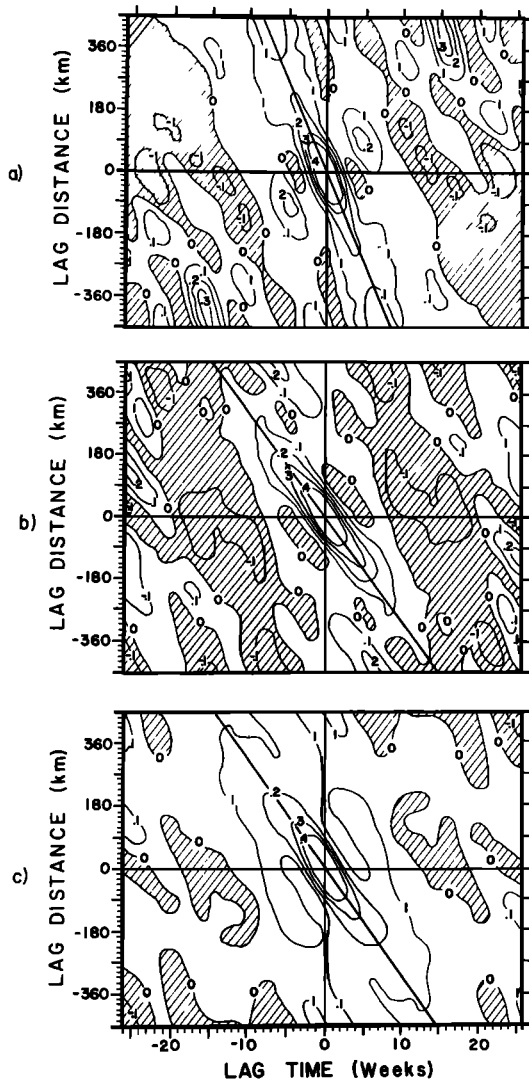


Fig. 11. Eddies. Space-time autocorrelation functions of normalized  $A_e$  for (a) year one, (b) year two, and (c) both-years. The average propagation speeds equal the slopes of the dark lines (see Table 2).

stantially dissipated while they were passing the region near Hudson Canyon. The average residence time for an eddy at any particular point along the shelf-slope front was between 2 and 3 weeks, averaging about 3 weeks to the northeast of Hudson Canyon and about 2.2 weeks to the southwest (Figure 10c). On the average, 1.2 eddies were visible each week along the front for year one, and 2.4 eddies were visible each week for year two (not shown).

**Correlation analyses.** The spatial and temporal correlation scales (Table 2) for the eddies were very similar to those of the shelf-slope front. The spatial correlation scale had a mean of 80 km for year one and 81 km for year two and both-years, and its standard deviation was 18 km for both-years. Hence the eddy diameter did not vary by more than about a factor of 2. The substantial increase in the temporal correlation scale from 1.9 weeks for year one to 2.6 weeks for year two is indicative of slower propagation during year two. The space-time autocorrelation function (Figure 11 and Table 3) showed similar temporal correlation scales but somewhat smaller spatial correlation scales. The ridges and troughs of this function were tilted and approximately parallel to each other, indicating the dominance of propagating perturbations. The av-

erage southwestward propagation speed decreased from 8 to 5 cm/s from year one to year two. It was 6 cm/s for both-years, which agrees with estimates by *Lai and Richardson* [1977].

From the space-time autocorrelation functions computed over subdomains for both-years (not shown) the average propagation speed was 4 cm/s along the western end of the Georges Bank and 7 cm/s along the Middle Atlantic Shelf to the south of Hudson Canyon. This result, plus the reduction to the southwest in the mean maximum  $A_e$  for all eddies (Figure 10b), confirms *Gotthardt's* [1973b] report that eddies tend to shrink and increase in speed as they propagate along the shelfbreak.

**Spectrum analyses.** The frequency autospectra for the three cases (Figure 12a) had significant peaks at periods between 6 and 8 weeks, about half the average time between the passage of successive eddies at any given point along the shelf. The wave number autospectrum (Figure 12b) had a significant peak at a wavelength of about 225 km, about twice the alongshelf scale of the eddies. The total variance increased from year one to year two in both frequency and wave number autospectra owing to the larger number of eddies. In the frequency domain the increase was about 25%. In the wave number domain the increase was largest for wavelengths greater than 150 km, up to 75% near a wavelength of 225 km.

The ordinary wave number–frequency autospectrum for both-years (Figure 13a) had a maximum ridge at negative wave numbers, indicating the dominance of southwestward propagation. Most of the variance was concentrated at wavelengths greater than 90 km and periods greater than three weeks. This broad wave number–frequency ridge was probably due to the variable intereddy space and time scales and to fluctuations in eddy propagation speeds. The total and propagating wave number–frequency autospectra were almost

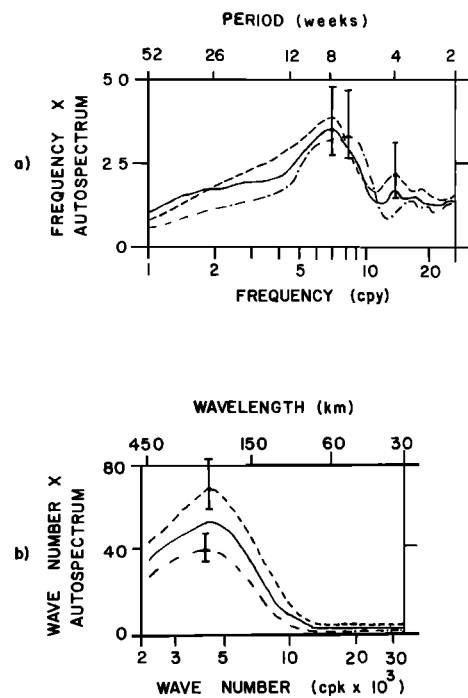


Fig. 12. Eddies. (a) Frequency autospectra (multiplied by  $\sigma$  to enhance the peaks) of normalized  $A_e$ , computed with 44 degrees of freedom. (b) Wave number autospectra (multiplied by  $k$  to enhance the peaks) of normalized  $A_e$ , computed with 200 degrees of freedom. The dash-dot curve is year one, the dashed curve is year two, and the solid curve is both-years.

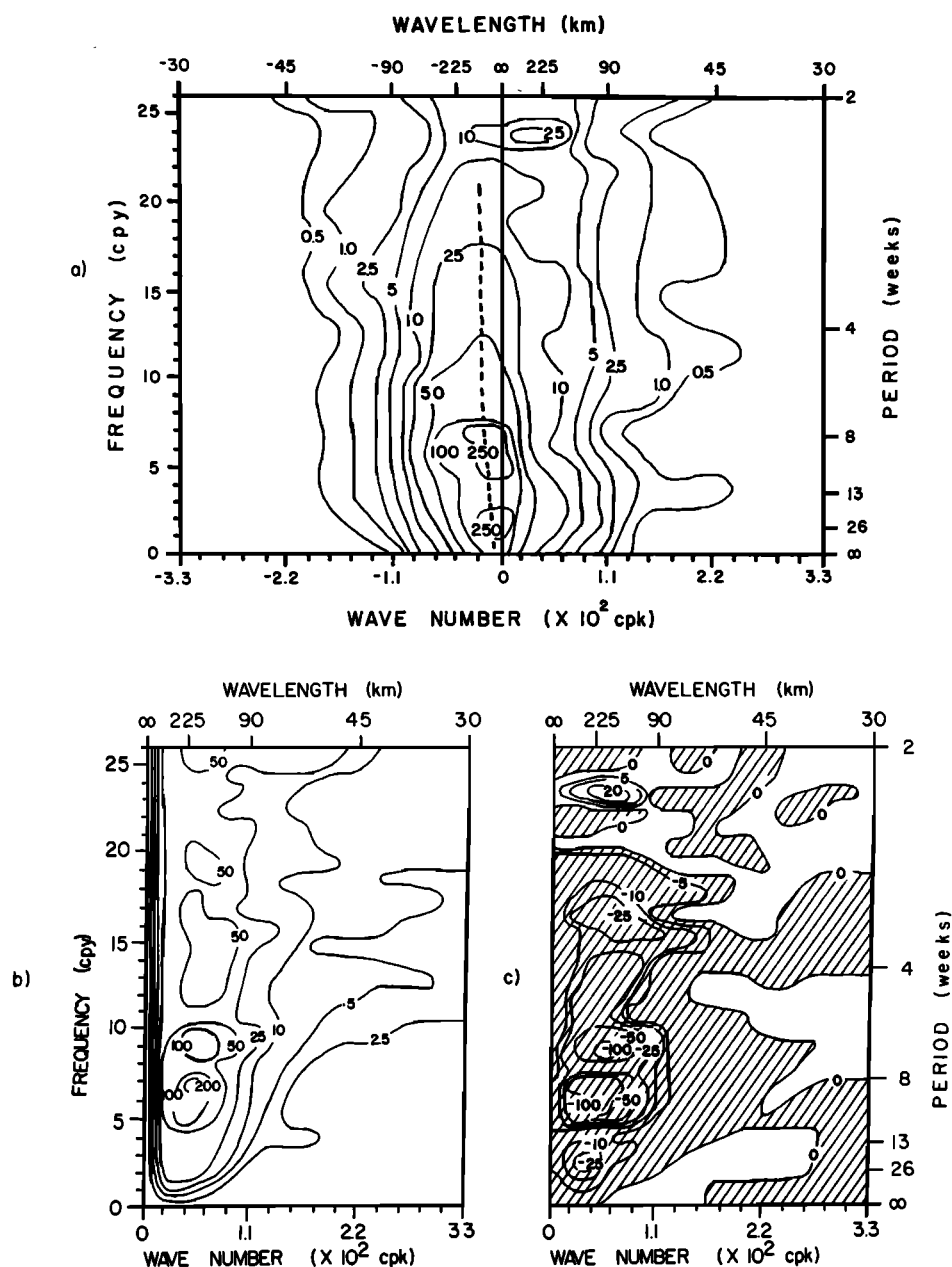


Fig. 13. Eddies. Wave number-frequency autospectra for both-years, computed with 12 degrees of freedom. (a) The ordinary autospectrum, where the dashed line denotes a maximum ridge. (b) The total autospectrum times  $10^4$  (multiplied by  $k$  and  $\sigma$  to enhance the peaks). (c) The propagating wave autospectrum, where shading indicates propagation toward negative  $y$ .

identical (Figures 13b and 13c); thus as is to be expected, the eddies' propagating variance was dominant. (Their standing wave variance was not analyzed.) Propagation speeds associated with the spectral peaks ranged between 1 and 20 cm/s (Table 5).

*Interaction with the shelf-slope front.* From the wave num-

TABLE 6. Predominant Scales of Interaction Between the Shelf-Slope Front and the Eddies

	$\lambda$ , km	$T$ , weeks	Speed, cm/s
Year 1	100 to -200	3.1-5.2	-2 to -11
Year 2	100 to -130	3.7-6.5	-2 to -6
Both-years	100 to -200	3.1-6.5	-2 to -11

The both-years case is based on Figure 14. Negative speeds correspond to southwestward propagation.

ber-frequency coherence squared (Figure 14), there were strong interactions between the shelf-slope front and the eddies for both-years. The most significant coherence occurred for negative  $k$ ; hence the interactions between the eddies and the front propagated mainly southwestward. The dominant interaction wavelength ranged between 100 and 200 km; the dominant interaction period ranged between 3 and 7 weeks (Table 6). The propagation speed of the dominant interactions was several centimeters per second to the southwest, consistent with the speed of both the eddies and the perturbations of the front. There were also unexpectedly coherent interactions for positive  $k$  at periods of 2-3 weeks and wavelengths of 30-45 km, which could be due to the response of both systems to northeastward propagating atmospheric disturbances or (less likely) to downstream propagating Gulf Stream meanders.

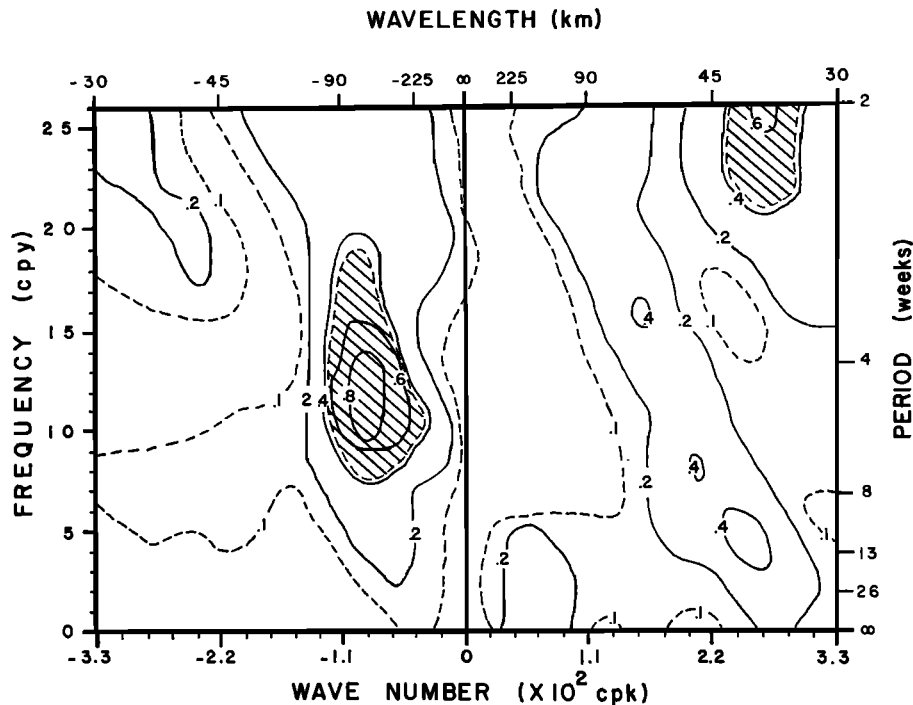


Fig. 14. Wave number–frequency coherence squared between the shelf-slope front and the eddies for both-years, computed with 12 degrees of freedom. Regions of significant coherence squared are shaded.

#### GULF STREAM FRONT

**Notable features.** On the basis of space-time contours of  $A_g$  the large-scale meanders propagated downstream, decreased in wavelength, and increased in amplitude [Halliwell, 1978]. The amplitudes of small-scale ( $\leq 150$  km) perturbations of the front were an order of magnitude smaller than those of the large-scale meanders. These perturbations were not resolved in the present study because they often appeared in the EOF charts for only 1 week.

**Statistics of  $A_g$ .** The mean position for both-years of the Gulf Stream front was concave seaward in the interval  $0 \leq y_g \leq 540$  km and straight for  $y_g > 540$  km (Figure 2). The standard deviation increased downstream from 25 km at  $y_g = 0$  km to 80 km at  $y_g = 810$  km. These values were very similar to those of the shelf-slope front. Within the interval  $0 \leq y_g \leq 630$  km, the mean position of the Gulf Stream front shifted shoreward during year two (Figure 15). The magnitude of this shift was 35 km at  $y_g = 0$  km, increasing to a maximum of 60 km at  $y_g = 360$  km (south of New England).

**Empirical orthogonal functions.** For both-years, about 90% of the total variance of the front was contained in the first five EOF modes (Figure 16), and the normalized entropy was 0.78 (Table 1). Since their normalized entropy was greater, the per-

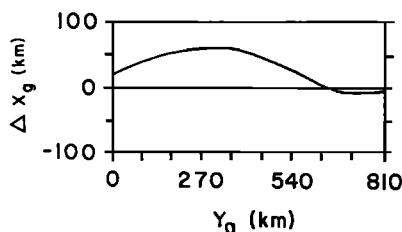


Fig. 15. Gulf Stream front: change in mean position between years one and two as a function of  $y_g$ .

turbations of the Gulf Stream front were less ordered than those of the shelf-slope front. The amplitudes of modes one, three, four, and five increased, and their wavelengths decreased, downstream. These four modes accounted for more than 70% of the total variance. The first five modes were most vigorous at frequencies less than 10 cpy. Mode two closely resembled the shift in the mean position of the front from year one to year two (Figure 15), and its spectrum was peaked at 1–4 cpy. The modes were very similar for years one and two [Halliwell, 1978]. The normalized entropy was 0.74 for years one and two (Table 1); thus the Stream had the same degree of order in each year.

**Correlation analysis.** The spatial and temporal correlation scales (Table 2) were comparable with those of the shelf-slope front and the eddies. (The  $A_g$  series were normalized before computing the correlation and spectrum functions to prevent the dominance of the large variance downstream. The normalization did not have a substantial effect on the space and time scales which dominate the correlation and spectrum functions.) The spatial correlation scale was  $92 \pm 42$  km for both-years. The large temporal variation of this scale was indicative of shifts between highly and slightly perturbed states of the Stream on a time scale of several weeks [Halliwell, 1978]. The spatial correlation scale often decreased to about 60 km; thus an alongstream sampling rate of 60 km is required to always resolve the dominant (low frequency) meanders. The temporal correlation scale was  $2.5 \pm 1.1$  weeks for both-years. The scale was 3–5 weeks in the interval  $0 \leq y_g \leq 450$  km and 1–2 weeks for  $y_g > 450$  km. Thus the temporal scale decreased substantially downstream, and sampling rates of 3 weeks within about 500 km downstream of Cape Hatteras and of 1 week farther downstream are required to resolve the dominant meanders. The temporal and spatial correlation scales were essentially identical for years one and two.

The correlation scales (Table 3) computed from the space-

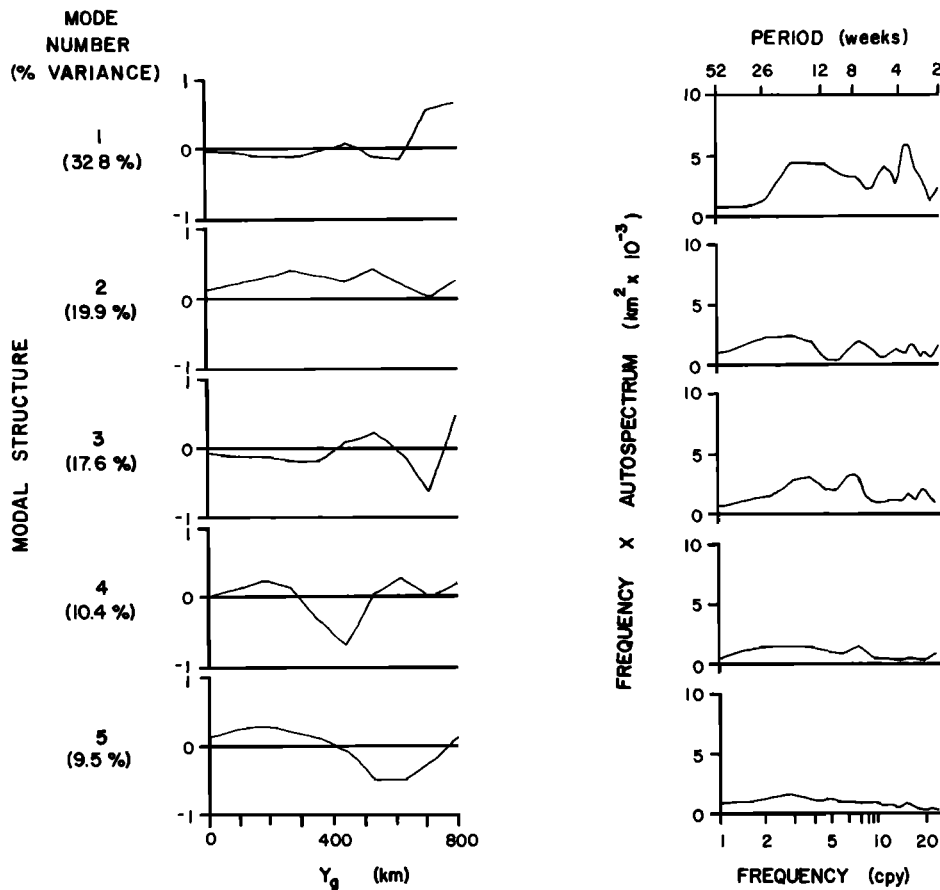


Fig. 16. Gulf Stream front: the five most significant EOF modes (modal structures and autospectra of the EOF amplitudes) for both-years.

time autocorrelation function (Figure 17) were similar to those discussed above. Downstream propagating disturbances were dominant. Their propagation speed averaged 6 cm/s during year one and 7 cm/s during year two and both-years. These speeds were similar to the speed (8 cm/s) reported by Hansen [1970] for the dominant meanders. During year two and both-years, there was also an indication of upstream propagation.

**Spectrum Analyses.** The frequency autospectra for the three cases (Figure 18a) had a significant peak near a period of 7 weeks for year two and both-years. During year two the amplitude of the frequency autospectrum was about 20% larger for periods less than about 20 weeks and about 40% larger near a period of 7 weeks. The frequency autospectra generally decreased as  $\sigma^{-1}$  except during year one for periods greater than 20 weeks. The wave number autospectra (Figure 18b) had broad peaks centered on a wavelength of 320 km. The amplitude increased about 15% during year two for wavelengths between 180 and 500 km. The functional dependence of the wave number autospectra on  $k$  was obscured by this large, broad peak. The dominant motions at 7 weeks and 320 km correspond to those reported by Hansen [1970].

The ordinary wave number–frequency autospectrum for both-years (Figure 19a) had a ridge at positive wave numbers and frequencies between 1 and 10 cpy, indicating the dominance of downstream-propagating meanders. The maximum occurred at a wavelength of 360 km between periods of 6 and 13 weeks and increased to 600 km at 52 weeks. The scales of the dominant spectral peaks of the total wave number–fre-

quency autospectra (Figure 19b) for the three cases are listed in Table 4. Broad spectral peaks occurred between wavelengths of 180 and 900 km and periods of 7 and 26 weeks (Table 4). A secondary spectral peak occurred for wavelengths less than 450 km and a period near 3 weeks during year two and both-years. (EOF mode one also had a spectral peak near 3 weeks.) Large variance for the smaller wavelengths and shorter periods may be due to aliasing by the small-scale meanders reported by Robinson *et al.* [1974]. The standing wave number–frequency autospectrum was significant for wavelengths between 180 and 900 km and periods of 5–26 weeks. The propagating wave number–frequency autospectrum was dominated by long-period ( $\geq 4$  weeks), downstream-propagating meanders (Figure 19c and Table 5). Their wavelength band was between 220 and 600 km for the three cases, and they had spectral peaks in two period bands: 6–10 and 17–52 weeks. Within the first band, the maximum was centered on a wavelength of 320 km and a period of 8 weeks, in agreement with Hansen [1970]. Waves with a period of 3–4 weeks also propagated downstream; they had somewhat shorter wavelengths, 200–300 km.

**Interactions with the shelf-slope front.** The maxima in the wave number–frequency coherence squared between the shelf-slope and Gulf Stream fronts (Figure 20) differed among the three cases. (Here,  $A_t$  was subsampled, so that  $A_t$  and  $A_s$  had a common sampling interval of  $\Delta y = 90$  km.) The coherence was generally larger for positive than for negative wave numbers due to the dominant influence of downstream-propagating Gulf Stream meanders on the shelf-slope front, and it

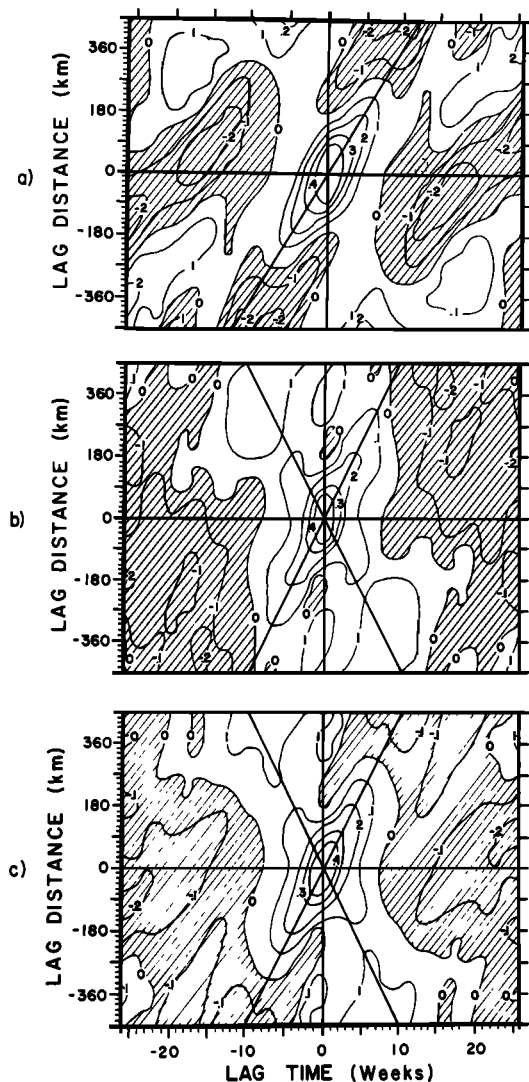


Fig. 17. Gulf Stream front: space-time autocorrelation functions of normalized  $A_g$  for (a) year one, (b) year two, (c) both-years. The average propagation speeds equal the slopes of the dark lines.

was generally larger for periods between 4 and 13 and between 2 and 3 weeks (Table 7).

#### DISCUSSION

Between Cape Charles and the Great South Channel, the shelf-slope front was bound to the shelfbreak except when eddies drove shelf water offshore. The front was spatially inhomogeneous between Cape Charles and the Northeast Channel because the space-time variability was different over the eastern end of Georges Bank than elsewhere. Along the eastern end of Georges Bank (and eastward along the Scotian Shelf) the front was not tightly bound to the shelfbreak, and it was frequently displaced more than 100 km seaward of the shelfbreak for several weeks. These large perturbations probably affected the shelf-slope water exchange processes of Georges Bank and the Scotian Shelf. (A complementary study of EOF charts has been initiated at the Bedford Institute of Oceanography for the Scotian Shelf east to the Grand Banks to more fully explore this regime (P. C. Smith, personal communication, 1978).) The front was apparently influenced by the numerous eddies and the vigorous meandering of the Gulf Stream to the south and east of the Bank. Its perturbations are

nonstationary because the amplitude of the temporal variability changed substantially between years one and two. For example, the large perturbations along Georges Bank were less intense, and the seaward perturbations forced by the eddies to the southwest of the Bank were more intense during year two than during year one.

Three components of the space-time variability of the shelf-slope front were resolved: long-period (several weeks), propagating perturbations forced by the eddies; long-period (>4 weeks), standing perturbations; and short-period (2–4 weeks), rapidly propagating (up to 50 cm/s to the southwest) waves. (There are important time scales of motion unresolved in this study; e.g., several-day (storm driven) and tidal motions. Though they have modest (>8 km) spatial resolution, the Goes IR images, available every 30 min, could help in this regard. However, the authors have not used the Goes images.) The perturbations forced seaward by the eddies had along-shelf scales of about 100–200 km, propagated southwestward at about 5 cm/s, and were more common and had larger amplitudes during year two. The low-frequency, standing wave perturbations were essentially 180° out of phase between the Middle Atlantic Shelf and the New England Shelf and Georges Bank. The long-wavelength, high-frequency, southwestward propagating perturbations may have resulted from the passive advection of the front due to coastally trapped waves. They were prominent only during year one, propagated at a speed of 7–50 cm/s, and had wavelengths between 70 and 600 km.

The shelf-slope front is generally treated, if at all, as a stationary offshore boundary for shelf water in models of shelf circulation. A complete model will presumably include the effects of the large frontal perturbations and the exchange forced by the eddies. There are interannual variations in the space-time variability, and presumably the concomitant cross-front exchange, which also need to be incorporated into models.

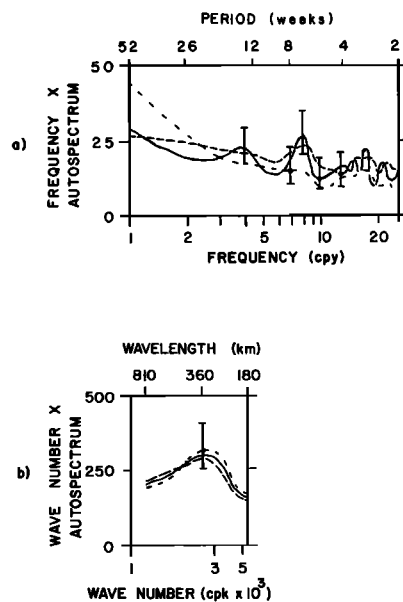


Fig. 18. Gulf Stream front. (a) Frequency autospectra (multiplied by  $\sigma$  to enhance the peaks) of normalized  $A_g$ , computed with 36 degrees of freedom. (b) Wave number autospectra (multiplied by  $k$  to enhance the peaks) of normalized  $A_g$ , computed with 160 degrees of freedom. The dash-dot curve is year one; the dashed curve is year two; and the solid curve is both-years.

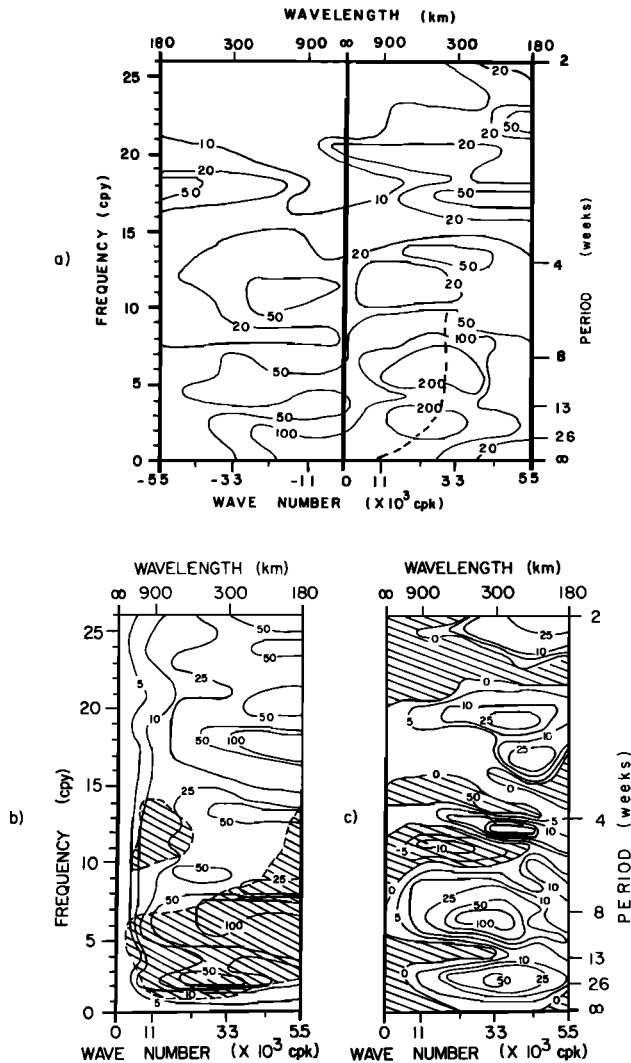


Fig. 19. Gulf Stream front: wave number-frequency autospectra for both-years, computed with 12 degrees of freedom. (a) The ordinary autospectrum, where the dashed line denotes a maximum ridge. (b) The total autospectrum times  $10^4$  (multiplied by  $k$  and  $\sigma$  to enhance the peaks), where the shading shows the regions in  $(k, \sigma)$  space in which a significant fraction of the total variance is due to standing waves. (c) The propagating wave autospectrum, where shading indicates propagation toward negative  $y_g$ .

Fourteen eddies, about equal to the number of dominant Gulf Stream meander cycles, influenced the circulation over the outer shelf and slope during both years, though only about half of them impacted any particular location along the shelf-break. Their mean diameter was about 100 km, and they propagated southwestward at an average speed of cm/s. Some had life spans exceeding half a year. Most formed 1,000 km or more, but none less than 500 km, downstream of Cape Hatteras. After contacting the continental slope (usually off Georges Bank), they propagated southwestward along the shelfbreak until they were captured by the Gulf Stream, generally near Cape Hatteras but sometimes south of New England or Georges Bank. They tended to decrease in diameter from about 120 to 90 km and increase in speed from 4 to 7 cm/s as they passed Hudson Canyon. From year one to year two their average speed along the shelfbreak decreased from 8 to 5 cm/s. An average of 3–5 eddies per year affected the front at any point along the shelf, and the eddies had an average

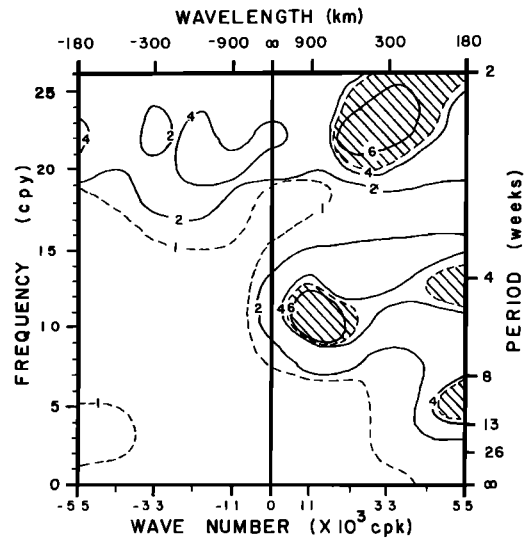


Fig. 20. Wave number-frequency coherence squared between the shelf-slope and Gulf Stream fronts for both-years, computed with 12 degrees of freedom. Regions of significant coherence squared are shaded.

residence time of 2–3 weeks, which agrees closely with *Lai and Richardson* [1977], *Gotthardt* [1973b], and *Bisagni* [1976]. Thus an eddy was present between 6 and 15 weeks per year at any location along the shelf. The emergence of a surface manifestation of an eddy at the shelf-slope front following the passage of Hurricane Belle raises the question of how many such eddies remain undetected due to the lack of a surface temperature manifestation in the summertime.

The Gulf Stream front had a spectral peak at a wavelength of about 320 km and a period of about 7–8 weeks, with an average downstream propagation speed of 6 cm/s, in close agreement with *Hansen* [1970]. Actually, the scales were broadbanded, with wavelengths between 220 and 600 km and two dominant period bands, between 6 and 10 weeks and between 17 and 52 weeks. The wavelengths decreased and amplitudes increased as the disturbances propagated downstream; thus the Stream's perturbations were spatially inhomogeneous. Some of the low-frequency variance of the Stream, for wavelengths between 180 and 900 km and periods between 7 and 52 weeks, was due to standing waves. Except for its mean position, the statistics of the Stream were essentially stationary over both-years, in contrast to those of the shelf-slope front. Despite the statistical similarities between years the Stream shed four eddies south of New England and Georges Bank during year two, much farther upstream than was typical during year one. These eddies, and those formed farther downstream during year two, vigorously entrained shelf water. After the severe winter of 1977, which corre-

TABLE 7. Predominant Scales of Interaction Between the Shelf-Slope and Gulf Stream Fronts

	$\lambda$ , km	$T$ , weeks	Speed, cm/s
Year 1	180–600	5.8–13	2–17
	180–900	2.0–24	7–74
Year 2	180–400	5.8–13	2–11
	180–900	2.0–3.7	8–74
Both-years	180–260	7.4–13	2–6
	180–900	4.0–6.5	5–37
	180–750	2.0–2.7	11–62

Both-years cases are based on Figure 20.

sponded to the second quarter of year two, the Gulf Stream transport was about 25% greater than its historical average and about 50% greater than the previous year [Worthington, 1977]. From the present study, the Stream also shifted shoreward south of New England, and shed more eddies, during the anomalous weather patterns of late 1976 and early 1977. (As a further indication of its disturbed state, the Gulf Stream variance along the South Atlantic Shelf was half a decade larger than usual during the late spring and summer of 1977, and the Stream was located as far shoreward as the 45-m isobath (I. J. Pietrafesa, personal communication, 1979).) Thus the shelf circulation may be indirectly driven by the large-scale atmospheric circulation through subtle relationships involving the number of eddies shed by the Gulf Stream and their influence on shelf circulation through entrainment and momentum and vorticity transfers.

Our results imply that the shelf-slope front should be sampled at alongfront intervals of no greater than 25 km and at least monthly along Georges Bank and weekly to the southwest of the Great South Channel. (These scales are quite similar to the correlation scales found in a synoptic field study of the shelf-slope front by Mooers *et al.* [1979].) Of course, greater temporal sampling rates are required to resolve the high-frequency perturbations reported by Voorhis *et al.* [1976] and Flagg [1977]. The Gulf Stream front should be sampled at alongfront intervals of no greater than 60 km and at least monthly within 500 km downstream of Cape Hatteras and weekly farther downstream to resolve the dominant meanders of the Stream. Again, greater temporal and spatial sampling rates are required to resolve the high-frequency meanders reported by Robinson *et al.* [1974].

The wave number-frequency spectra of oceanic synoptic scale phenomena presented yield sampling rate information needed for designing process experiments and ocean monitoring programs. They also provide information on the dominant time and space scales of interactions between the Gulf Stream and shelf-slope fronts and between the eddies and the shelf-slope front. The methods of analysis used here could probably be extended to evaluate theories for Gulf Stream and shelf-slope front instabilities. In more general terms, the space-time series derived from the satellite thermal imagery are potent tools for monitoring long-term (seasonal and interannual) variability of major components of the Middle Atlantic Shelf, Georges Bank, and Scotian Shelf circulation and that of the Northwest Atlantic, as well as their synoptic scale variability and its interannual variations. Obviously, they would be even more valuable if they were integrated with thermal and visible imagery from other satellite systems, satellite altimetry data, shipboard hydrographic data, and other data sets. In the next phase of our studies, we anticipate working with longer space and time series, higher spatial resolution for the Gulf Stream front, and space-time series of sea level and atmospheric forcing data, with which we should be able to perform a response analysis of the shelf circulation due to the predominant forcing functions. When the oceanographic community becomes more familiar with the type of data analyzed here and its dynamical information content, such remote sensing data can probably be used for boundary data in numerical forecast models of at least shelf circulation.

*Acknowledgments.* This research was supported under subcontract #46499 from the EG&G Environmental Consultants (Richard C. Scarlet) as part of the New England Outer Continental Shelf Physical

Oceanography Program sponsored by the Bureau of Land Management, U.S. Department of Interior. R. W. James and R. J. Perchal generously supplied the EOFA charts which made this study possible, and Perchal provided helpful discussions on his method of chart preparation and comments on a draft of the manuscript. M. C. Ingham and J. T. Gunn made available their statistical results for the shelf-slope surface front position, and C. N. Flagg provided a copy of his dissertation at an early date. Bruce Lee provided helpful editorial suggestions. Anonymous referees noted some faulty logic related to the discussion of Hurricane Belle and provoked a streamlining of the text.

## REFERENCES

- Beardsley, R. C., and C. N. Flagg, The water structure, mean currents, and shelf water/slope water front of the New England continental shelf, *Mem. Soc. Roy. Sci. Liege*, 10, 209–225, 1976.
- Bendat, J. S., and A. C. Piersol, *Random Data: Analysis and Measurement Techniques*, 407 pp., John Wiley, New York, 1971.
- Bisagni, J. J., Anticyclonic Gulf Stream eddies in the western North Atlantic Ocean, 1974–1975, and their passage through Deepwater Dumpsite 106, *Dumpsite Eval. Rep. 76(1)*, Nat. Oceanic and Atmos. Admin., Washington, D. C., 1976.
- Chamberlin, J. L., Bottom temperatures on the continental shelf and slope south of New England during 1974, in *The Environment of the United States Living Marine Resources—1974*, *Marmap Contrib. 104*, edited by J. R. Goulet, Jr., chap. 18, pp. 1–13, National Marine Fisheries Service, Washington, D. C., 1976.
- Davis, R. E., Predictability of sea surface temperature and sea level pressure anomalies over the north Pacific Ocean, *J. Phys. Oceanogr.*, 6, 249–266, 1976.
- Flagg, C. N., The kinematics and dynamics of the New England continental shelf and shelf/slope front, Ph.D. dissertation, 207 pp., Mass. Inst. of Technol. and Woods Hole Oceanogr. Inst., 1977.
- Gotthardt, G. A., Observed formation of a Gulf Stream anticyclonic eddy, *J. Phys. Oceanogr.*, 3, 237–238, 1973a.
- Gotthardt, G. A., Gulf Stream eddies in the western North Atlantic, *Tech. Note 6150-16-73*, 42 pp., U.S. Nav. Oceanogr. Office, Washington, D. C., 1973b.
- Gotthardt, F. A., and G. I. Potocsky, Life cycle of a Gulf Stream anticyclonic eddy observed from several oceanographic platforms, *J. Phys. Oceanogr.*, 4, 131–134, 1974.
- Gunn, J. T., Variations in the position of the shelf water front off the Atlantic coast between Georges Bank and Cape Romain in 1976, in *Ocean Variability: Effects on U. S. Marine Fishery Resources—1976*, *Marmap Contrib.* edited by J. R. Goulet, Jr., and E. D. Haynes, pp. 299–312, National Marine Fisheries Service, Washington, D. C., 1979.
- Halliwel, G. R., Jr., The space-time structure and variability of the shelf water/slope water and Gulf Stream surface thermal fronts, and warm-core eddies, off the northeast U. S., *Tech. Rep. CMS-C-2-78*, 195 pp., Coll. of Mar. Stud., Univ. of Del., Lewes, 1978.
- Hansen, D. V., Gulf Stream meanders between Cape Hatteras and the Grand Banks, *Deep Sea Res.*, 17, 495–511, 1970.
- Ingham, M. C., Variation in the shelf water front off the Atlantic coast between Cape Hatteras and Georges Bank, in *The Environment of the United States Living Marine Resources—1974*, *Marmap Contrib. 104*, edited by J. R. Goulet, Jr., chap. 17, pp. 1–21, National Marine Fisheries Service, Washington, D. C., 1976.
- Inspersen, W., Representation of meteorological variables by empirical orthogonal functions, in *Statistical Methods and Instrumentation in Geophysics*, pp. 109–114, Teknologisk, Oslo, 1971.
- Lai, D. Y., and P. L. Richardson, Distribution and movement of Gulf Stream rings, *J. Phys. Oceanogr.*, 7, 670–683, 1977.
- Maul, G. A., P. W. deWitt, A. Yanaway, and S. R. Baig, Geostationary satellite observations of Gulf Stream meanders: Infrared measurements and time series analysis, *J. Geophys. Res.*, 83, 6123–6135, 1978.
- Mooers, C. N. K., R. W. Garvine, and W. W. Martin, Summertime synoptic variability of the Middle Atlantic shelf water/slope water front, *J. Geophys. Res.*, 84, 4837–4854, 1979.
- Morgan, C. W., and J. M. Bishop, An example of Gulf Stream eddy-induced water exchange in the Mid-Atlantic Bight, *J. Phys. Oceanogr.*, 7, 472–479, 1977.
- O'Neill, E. L., *Introduction to Statistical Optics*, 178 pp., Addison-Wesley, Reading, Mass., 1963.
- Perchal, R. J., Satellite imagery of an anticyclonic eddy, *Gulfstream*, 1(12), 6–7, 1975.

- Perchal, R. J., Comparison of Gulf Stream edges detected by airborne radiation thermometer and VHRR-IR satellite imagery during Subaswex 1-76, *Tech. Note 3700-52-76*, 21 pp., U.S. Nav. Oceanogr. Office, Washington, D. C., 1976.
- Pratt, R. W., The interpretation of space-time spectral quantities, *J. Atmos. Sci.*, 23, 1060-1066, 1976.
- Robinson, A. R., J. R. Luyten, and F. C. Fuglister, Transient Gulf Stream meandering, I, An observational experiment, *J. Phys. Oceanogr.*, 4, 237-255, 1974.
- Saunders, P. M., Anticyclonic eddies formed from shoreward meanders of the Gulf Stream, *Deep Sea Res.*, 18, 1207-1219, 1971.
- Stumpf, H. G., and P. K. Rao, Evolution of Gulf Stream eddies as seen in satellite infrared imagery, *J. Phys. Oceanogr.*, 5, 388-393, 1975.
- U.S. Naval Oceanographic Office, Experimental ocean frontal analysis charts, Washington, D. C., 1975-1977.
- Voorhis, A. D., D. C. Webb, and R. C. Millard, Current structure and mixing in the shelf/slope water front south of New England, *J. Geophys. Res.*, 81, 3695-3708, 1976.
- Wang, D.-P., and C. N. K. Mooers, Coastal-trapped waves in a continuously stratified ocean, *J. Phys. Oceanogr.*, 6, 853-863, 1976.
- Worthington, L. V., Intensification of the Gulf Stream after the winter of 1976-77, *Nature*, 270, 415-417, 1977.
- Wright, W. R., The limits of shelf water south of Cape Cod, 1941-1972, *J. Mar. Res.*, 34, 1-14, 1976.

(Received August 11, 1978;  
revised June 28, 1979;  
accepted July 2, 1979.)